TAMPEREEN TEKNILLINEN YLIOPISTO
TAMPERE UNIVERSITY OF TECHNOLOGY

MARI PARTANEN

APPLICATION OF DIFFUSION-WEIGHTED MAGNETIC RESONANCE IMAGING IN DUCTAL BREAST CARCINOMA

Master of Science Thesis

Examiners: Professor Hannu Eskola
and Lic.Sc Ullamari Hakulinen
Examiners and topic approved by
the Council of the Faculty of Natural
Sciences on 7th of MAY 2014

ABSTRACT

TAMPERE UNIVERSITY OF TECHNOLOGY
Master's Degree Programme in Science and Engineering
PARTANEN, MARI: Application of Diffusion-Weighted Magnetic Resonance Imaging in Ductal Breast Carcinoma
Master of Science Thesis, 51 pages
APRIL 2015
Major: Advanced Engineering Physics
Examiners: Professor Hannu Eskola and Lic.Sc Ullamari Hakulinen
Keywords: Magnetic resonance imaging, Diffusion, Diffusion-weighted imaging, Breast cancer, Ductal carcinoma in situ

Diffusion-weighted imaging (DWI) is a novel magnetic resonance imaging (MRI) technique sensitive to Brownian motion. With the use of diffusion-sensitizing gradient pulses DWI enables the detection of microscopic diffusion of water molecules in biological tissues. Diffusion state for different voxels can be calculated from DW images with different diffusion weightings, resulting a quantitative apparent diffusion coefficient (ADC) map. Different tissues restrict diffusion in different ways, which makes DWI sensitive for alterations in movement of water molecules in normal versus abnormal tissue. So far DWI has been used clinically mainly for imaging brain disorders but applications on oncology are also promising. Breast cancer imaging is one potential application for DW imaging. The ADC values of malign breast lesions are usually lower than those of benign lesions, which makes DWI a potential tool for differentiating lesion types. DWI has multiple advantages over conventional contrast-enhanced MRI, for example it is cheaper and faster than DCE-MRI and to top it all it increases the sensitivity of breast lesion characterization.

In this Master of Science thesis 45 patients with 48 ductal carcinoma and 8 benign lesions were examined through four different studies: comparison of mean ADC values of benign and malign breast lesions, repeatability of ADC measurements, correlation between ADC values and Signal-to-Noise ratio and effect of lesions size to the ADC values. The statistical significance of the results was analyzed with statistical tests with *SPSS software*.

The normalized mean ADC values for benign lesions was found $0.80 \pm 0.23 \times 10^{-3}$ mm^2/s and for malign lesions $0.63 \pm 0.20 \times 10^{-3}$ mm^2/s and they were found significantly different. The cutoff value for malign lesions was determined 0.83×10^{-3} mm^2/s with sensitivity of 83.3% and specificity of 37.3%. The measurement method showed excellent repeatability (ICC 0.94), especially with big lesions. ADC and SNR values did not have significant correlation. These results were promising and they give a basis for further studies, like for studies with larger sample size and with several different malign lesion types. In the future the cutoff value of malign and benign lesions could be used as guidance tool for doctors in breast lesion characterization.

TIIVISTELMÄ

TAMPEREEN TEKNILLINEN YLIOPISTO
Teknisluonnontieteellinen koulutusohjelma
PARTANEN, MARI: Application of Diffusion-Weighted Magnetic Resonance Imaging in Ductal Breast Carcinoma
Diplomityö, 51 sivua
Huhtikuu 2015
Pääaine: Teknillinen fysiikka
Tarkastajat: professori Hannu Eskola, TkL Ullamari Hakulinen
Avainsanat: Magneettikuvaus, Diffuusio, Diffuusio-painotettu magneettikuvaus, Rintasyöpä, Ductal carcinoma in situ

Diffuusio-painotettu magneettikuvantaminen (Diffusion-Weighted Imaging, DWI) on uudenlainen lääketieteellinen kuvantamismenetelmä, joka perustuu vesimolekyylien Brownian liikkeeseen. DWI-tekniikka käyttää erityisiä herkistyspulsseja mitatessaan vesimolekyylien diffuusiota biologisissa kudoksissa. Diffuusion voimakkuutta eri kuva-alkioissa voidaan kuvata näennäisdiffuusiovakioilla (Apparent Diffusion Coefficient, ADC), joista voidaan muodostaa ADC-karttoja. ADC-kartat ovat lääketieteellisiä kuvia, joiden muodostamiseen käytetään kahta tai useampaa eri herkistyspulsseilla saatua diffuusiopainotettua kuvaa. Eri kudokset rajoittavat vesimolekyylien diffuusiota eri tavoin, mikä tekee DWI-tekniikasta herkän kudosten rakenne-eroille. Toistaiseksi DWI-tekniikan kliinisenä käyttökohteena ovat olleen erilaiset aivojen sairaudet. Menetelmällä on myös sovelluskohteita onkologiassa, erityisesti rintasyövän kuvantamisessa. Malignien kasvaimien ADC arvot ovat yleensä matalampia kuin vastaavat benignien kasvaimien arvot. DW-kuvantamisella on monia etuja tavalliseen varjoaine-magneettikuvantamiseen verrattuna: DWI on edullisempi ja nopeampi ja lisäksi se parantaa magneettikuvantamisen sensitiivisyyttä rintasyöpätyypin karakterisoinnissa.

Tämän diplomityön aineisto koostui 45 rintasyöpäpotilaasta, joilla oli yhteensä 48 malignia ja 8 benigniä kasvainta. Työssä suoritettiin seuraavat kokeet: benignien ja malignien kasvaimien ADC-keskiarvojen vertailu, ADC-mittausten toistettavuus, signaali-kohinasuhteen (SNR) ja ADC-arvojen välinen korrelaatio sekä kasvaimen koon vaikutus ADC-arvoihin. Tulosten tilastollista merkitsevyyttä analysoitiin *SPSS*-ohjelmalla.

Benignien kasvaimien normalisoiduksi ADC-arvoksi saatiin $0.80 \pm 0.23 \times 10^{-3}$ mm^2/s ja malignien vastaavasti $0.63 \pm 0.20 \times 10^{-3}$ mm^2/s ja ne todettiin eroavan tilastollisesti merkittävästi toisistaan. Malignien kasvaimien raja-arvoksi määritettiin 0.83×10^{-3} mm^2/s, jolloin sensitiivisyys oli 83.3% ja spesifisyys 37.3%. ADC-arvojen mittausmenetelmä osoitti eriomaista toistettavuutta (ICC 0.94), erityisesti suurien kasvaimien tapauksessa. ADC- ja SNR-arvojen välillä ei havaittu korrelaatiota. Tulokset olivat lupaavia, joten lisätutkimukset ovat perusteltuja. Esimerkiksi tutkimukset suuremmalla aineistolla ja eri rintasyöpätyyppien kanssa olisivat mielenkiintoisia. Tulevaisuudessa malignien ja benignien kasvaimien ADC-raja-arvoa voidaan käyttää radiologien työkaluna rintasyövän karakterisoinnissa.

PREFACE

This Master of Science Thesis was made at Tampere University of Technology at Biomedical Engineering Department. The clinical research was done at Tampere University Hospital during years 2014-2015. The examiners of the project were Professor Hannu Eskola and L.Sc. Ullamari Hakulinen. Materials used in this thesis were imagined in Turku University Hospital and collected by doctors Ilkka Koskivuo and Nina Brück during years 2011-2013. The contact person between materials and this thesis project was Professor Riitta Parkkola.

I would like to thank Hannu Eskola for offering interesting thesis topic and all the guidance provided through the project. I want thank Riitta Parkkola for help in designing the measurement procedure and all the guidance in this thesis. I want also thank Ullamari Hakulinen for all the help and support during the project. Million thanks for all the encouragement and conversations!

The support from outside this thesis project was equally important. I would like to thank the “optics team” (Liisa, Elisa, Jan, and Mikko) for all the support. And special thanks to my “savo team” (Enni and Tiina) for all the relaxing moments! And of course greetings for Kuopio for all the encouragement during the years! And last but not least I would like to thank from all my heart my Pekka for ALL the support. You have seen all the highs and lows during this project. Thank you for understanding and encouragement.

Tampere 23.3.2015

Mari Partanen

TABLE OF CONTENTS

ACRONYMS

ADC	Apparent Diffusion Coefficient
DCE-MRI	Dynamic Contrast-Enhanced Magnetic Resonance Imaging
DCIS	Ductal Carcinoma in Situ
DTI	Diffusion Tensor Imaging
DWI	Diffusion-Weighted Imaging
FID	Free Induction Decay
GE	Gradient Echo
ICC	Intra-Class Correlation
IDC	Invasive Ductal Carcinoma
ILC	Invasive Lobular Carcinoma
LCIS	Lobular Carcinoma in situ
MRI	Magnetic Resonance Imaging
NMR	Nuclear Magnetic Resonance
PGSE	Pulsed Gradient Spin Echo
RF	Radiofrequency
ROI	Region of Interest
SD	Standard Deviation
SE	Spin Echo
SNR	Signal-to-Noise Ratio
US	Ultrasound

LIST OF SYMBOLS

Mathematical notations

$\overline{v}$	vector
$\overline{V}$	matrix or tensor

Symbols

γ	gyromagnetic ratio
δ	gradient pulse duration
ζ	viscous friction coefficient
μ	mean
η	viscosity of fluid
π	pi
ω	angular frequency
Δ	time separation between gradient pulses, or difference in general
b	b-value
B	magnetic field strength
c	concentration
D	diffusion constant
$F_n(x)$	cumulative frequency sum
G	gradient strength
H	hypothesis
j	particle flux
k_B	Boltzmann constant
L	length
M	magnetization
n	sample size
N	number of for example molecules
r	displacement
R	radius
S	intensity
t	time
T	temperature
T_1	longitudinal relaxation
T_2	transverse relaxation

1. INTRODUCTION

Magnetic resonance imaging (MRI) is one of the most important imaging modalities in today's modern world. It has high contrast sensitivity to soft tissue differences and the use of nonionizing radiation makes it safe to use. MRI is based on *nuclear magnetic moment* of the hydrogen nuclei (protons). [1] When placed in high magnetic field protons align with parallel or antiparallel direction with the external magnetic field. *Radiofrequency* fields are used to excite the protons and after the pulse is switched off the system relaxes back to equilibrium state. When relaxing, protons are moving and moving charge generates a magnetic field. According to *Faraday's law of induction*, this induces a voltage that can be measured with MRI detectors. [2]

New technological advances in MRI have made possible the detection of microscopic diffusion of water molecules in extracellular space. This technique is called diffusion-weighted magnetic resonance imaging, or *diffusion-weighted imaging* (DWI). The MRI sequence sensitive for motion of water molecules was introduced by Stejskal and Tanner already in 1965. [3]

The level of diffusion in biological tissues is related to the tissue composition so it can be used as imaging contrast. With the obtained *diffusion-weighted images* (DW images) it is possible to generate diffusion constant maps, called *ADC maps*. ADC maps describe the strength of diffusion in tissues and they can be used to study abnormalities in tissue structures. DWI have been clinically used to detect brain disorders, like brain ischemia, but now also oncological applications are found potential. Breast cancer is one promising application for DW imaging. [3]

Breast cancer is the most common cancer type among women and it has come more and more frequent during last decades [4]. Cancer begins when cells in a part of the body start to grow out of control. In most cases the cancer cells form a tumor, which can be considered as *malign* or *benign* depending if it is cancerous or noncancerous, respectively. Malign changes are usually fast-growing lesions and they can spread to other parts of the body, which is called *metastasis*. Benign lesions instead do not invade into surrounding tissues nor form metastases. [5] Malign and benign changes can be further divided into subgroups. For example malign breast cancers can be into two main groups according to the appearance of growth: ductal and lobular carcinoma. [6] In this thesis the ductal carcinoma is studied.

Breast imaging is needed for different purposes, for example in screening for breast cancer and classifying breast abnormalities. Mammography is the most applied breast imaging method. Other used methods are *ultrasound* and MRI, which are usually used as additional methods for mammography [6]. DWI has potential to improve the

sensitivity of MR imaging. The contrast imaging without added contrast material is safer for patients and also cheaper and faster compared to DCE-MRI. [7]

This Master of Science Thesis is made at Tampere University of Technology at Biomedical Engineering Department. The clinical research is done at Tampere University Hospital. The purpose of this thesis is to measure and analyse ADC values of benign and malign breast lesions. The ADC values are analysed through four different studies: comparison of mean ADC values of benign and malign lesions, repeatability of ADC measurements, correlation between ADC and signal-to-noise ratio values and effect of lesions size to ADC values. Results are analysed statistically with *SPSS software*.

Thesis begins with technical and medical backgrounds, after which the used materials and methods are explained. Next the results of studies are first introduced and then discussed. Also reliability and clinical applicability of the DWI as breast imaging method are discussed. Finally conclusion ends the thesis.

2. MAGNETIC RESONANCE IMAGING

Magnetic resonance imaging (MRI) is a medical imaging technique based on the nuclear magnetic resonance (NMR). The main signal source is nuclei of hydrogen atoms ^1H, which are protons. NMR was invented already in 1920s but its medical potential was found in 1972 when *Raymond Damadian* measured MR signals from normal and tumor tissues of rats. The first MRI equipment prototype was developed in the *University of Aberdeen* (England) by *Jim Hutchison, Bill Edelstein*, and their colleagues. Nowadays MRI is widely used in hospitals for high resolution medical imaging. [8]

The magnetic imaging system requires three different kinds of electromagnetic fields: constant magnetic field, radiofrequency (RF) pulses, and gradient fields. The constant strong magnetic field is usually obtained with superconducting magnets and common clinical field strength is from 1.5 to 3 T. RF pulses are needed to excite and detect the MR signal. Moreover, magnetic field gradients are needed to be able to localize the MR signals in the body. These gradients are achieved by generating short-term spatial variations in magnetic fields strength across the patient. The gradient fields are needed in all three coordinate directions. [2; 9]

2.1 Nuclear magnetic resonance

The magnetic properties of the nuclei are described by the *nuclear magnetic moment*. The nuclear magnetic moment is generated by the protons and neutrons of the nucleus. If the number of protons, neutrons, or both is unpaired, the resultant noninteger spin generates a nuclear magnetic moment. Otherwise no net nuclear magnetic moment is observed. The nucleus of the hydrogen atom is composed of a single proton, which thus has a nonzero nuclear magnetic moment. Hydrogen is a good choice for clinical use in MRI because it has large magnetic moment, magnitudes of greater sensitivity compared to other elements and it has also great abundance in biological tissues. The nuclear magnetic moment of a single atom is not strong enough to be observed, but a large number of nonrandomly oriented nuclei generates a detectable nuclear magnetic moment, from which the MRI signals are derived. [2; 9]

Proton spins around its own axes, and thus the hydrogen nucleus is a continuously rotating positive charge. The moving charge generates a magnetic field, so the proton can be considered as a tiny bar magnet. When placed in a strong magnetic field B_0, the proton tries to align itself parallel with the external field. However, the proton experiences a turning force, *torque*, which prevents the proton to align completely with the external field. This makes the proton to *precess* around the direction of the ex-

ternal magnetic field (Fig. 1a). The precession occurs at an angular frequency ω_0 which is proportional to the external magnetic field B, given by the *Larmor equation*:

$$\omega_0 = \gamma B, \tag{1}$$

where γ is the *gyromagnetic ratio* unique for each element. [2; 9]

2.2 Magnetization

When placed in external magnetic field B, some of the protons align in *parallel* and some in *antiparallel* direction with the field due to the magnetic forces (Fig. 1a). At equilibrium the occupation of the states is almost equal but a slight majority exist in the low energy level, which means the parallel direction with the applied field. Although the difference in the occupation of the two energy levels is quite small, it is enough to produce a detectable MRI signal. The vector sum of all the spins generates the net *magnetization* M, which is aligned with the external magnetic field B (Fig. 1b). The magnetization vector M does not have a component in the perpendicular direction because the spins are randomly distributed over the surface of the cone, and thus sum to zero. [2; 9]

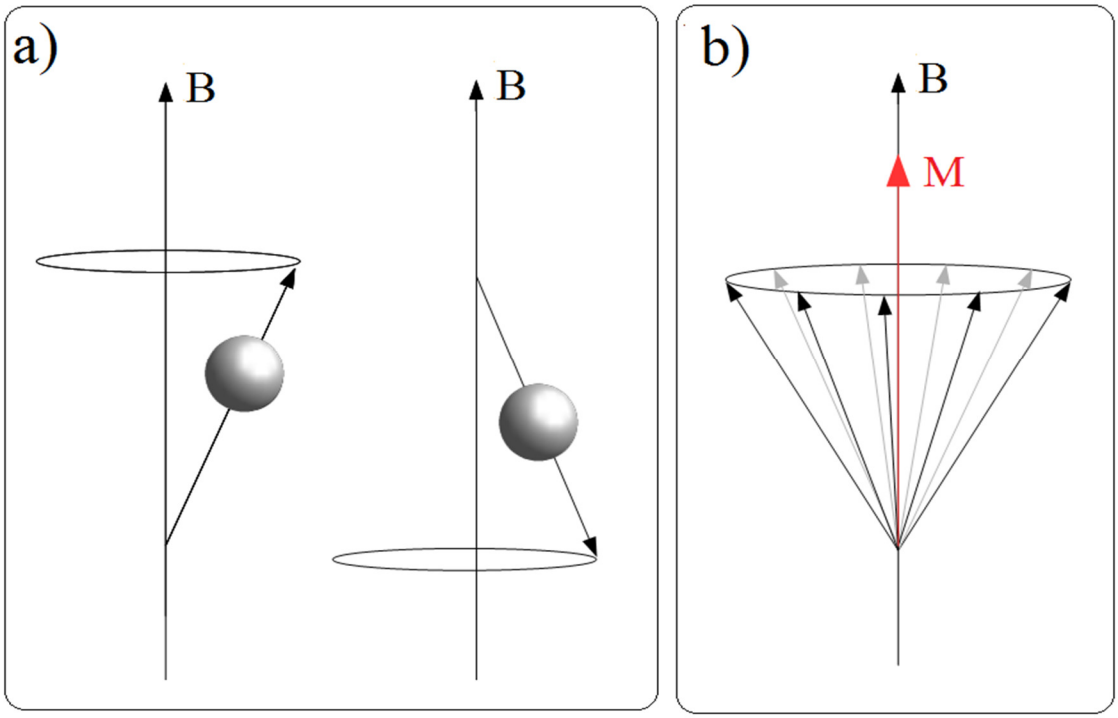

Figure 1. a) A single proton can precess about its axis in parallel or antiparallel direction with respect to the external magnetic field B. b) A group of protons generates the net magnetization M. Figure modified from *MRI From Picture to Proton* [9].

2.3 Image acquisition

Magnetization M is the order of microtesla, so it is really small compared to the main magnetic field [9]. In order to get a measurable signal with MRI, the spins are excited with RF pulses oscillating at the Larmor frequency.

2.3.1 Excitation

The magnetization vector M can be tilted to the transverse plane using a RF pulse oscillating at the Larmor frequency. This Larmor resonance frequency pulse excites protons from lower energy state (the parallel direction) to the higher energy state (the antiparallel direction), and the magnetization vector z-axis component, the *longitudinal magnetization* M_z along the direction of the main magnetic field, decreases. Respectively the *transverse magnetization* M_{xy} increases. M moves away from the z-axis until the RF pulse is switched off. With a 90° RF pulse the magnetization vector M can be turned to the xy-plane, and thus M_z reaches 0 value. (Fig 2) After this the magnetization will relax back to original state. [2; 10]

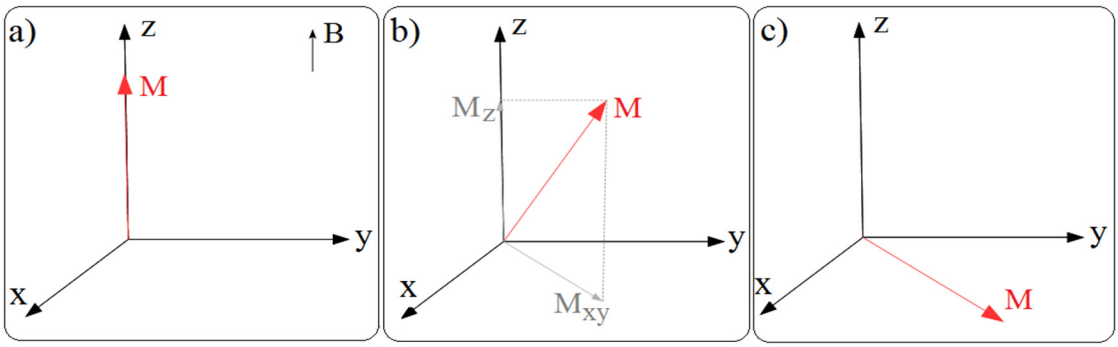

Figure 2. a) In equilibrium the magnetization vector M is aligned with external magnetic field B in z-direction. b) When 90° degree RF pulse is applied to the system, magnetization vector M starts to move away from z-axis. Longitudinal magnetization M_z presents the z-component of the magnetization vector M and respectively transverse magnetization M_{xy} describes the magnetization vector's component in xy-plane. c) 90° RF pulse will turn the magnetization vector M into the xy-plane.

2.3.2 Relaxation

An applied RF pulse creates a non-equilibrium state by adding energy to the system and so after the pulse is switched off the system relaxes back to the thermal equilibrium. There are two principal relaxation processes: *spin-lattice* (T_1) and *spin-spin* (T_2) relaxations. These can be described mathematically with set of differential equations which are called *Bloch equations*. [9; 10]

Spin-lattice relaxation T_1, also called as *longitudinal relaxation*, describes the rate of recovery of the longitudinal magnetization M_z towards the equilibrium after the

RF pulse has been switched off. T_1 describes the time needed for 63% (1-(1/e)) recovery. The recovery of magnetization as a function of time is described as follows:

$$M_z(t) = M_0\left(1 - e^{-t/T_1}\right) + M_z(0)e^{-t/T_1}, \quad (2)$$

where M_0 is the equilibrium magnetization.

Spin-spin relaxation, also called as *transverse relaxation* T_2, instead describes the dephasing of spins, which leads to signal decay. Elapsed time between the peak transverse signal and 37% (1/e) of the peak level is the T_2 relaxation time. Mathematically this is described as:

$$M_{xy}(t) = M_{xy}(0)e^{-t/T_2}\,. \quad (3)$$

Different tissues have different values for T_1 and T_2 time constants and thus different recoveries, which gives rise to contrast in MR images. In Figure 3 the equations (2) and (3) are plotted against time. [10; 11]

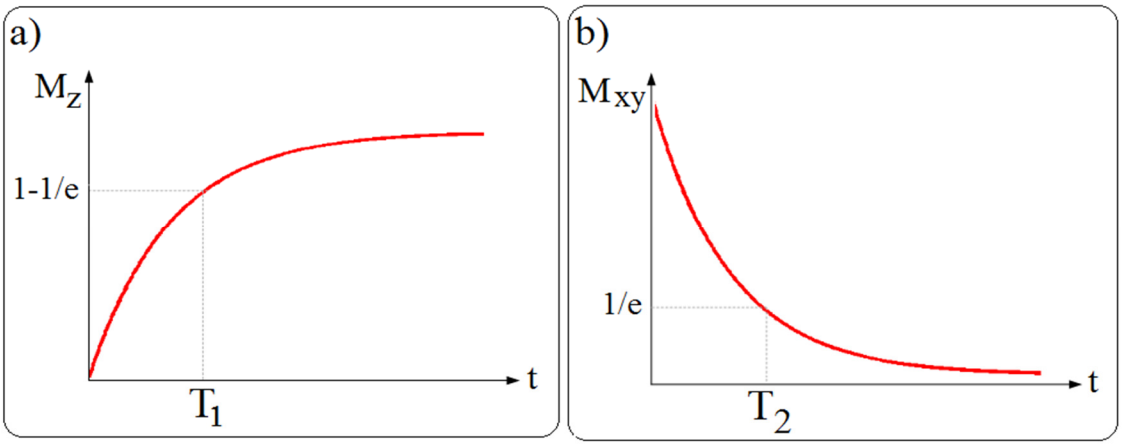

Figure 3. a) After 90° pulse the longitudinal magnetization M_z will return to equilibrium exponentially. At $t=T_1$ the longitudinal magnetization M_z has recovered by factor 1-(1/e). b) The loss of transverse magnetization M_{xy} phase coherence occurs exponentially caused by intrinsic spin-spin interactions. At $t=T_2$ the signal has decayed to 1/e of the initial transverse magnetization.

When a RF pulse is applied to the system, magnetization vector rotates into the transverse plane. In the transverse plane the precessing magnetization will generate a time-varying magnetic flux. According to *Faraday's law of induction*, this flux induces a voltage that can be measured with MRI detectors. The amplitude of the signal decays exponentially to zero rapidly, because the protons dephase with respect to each other. This decay signal is called *Free Induction Decay* (FID). However, FID is not used to generate MR images, instead different kinds of pulse sequences are used in clinical scans. [9; 10]

2.4 Pulse sequences

The RF pulse sequences applied to the system are called pulse sequences. There are two common pulse types used in clinical use: *spin echo* (SE) and *gradient echo* (GE) sequences. In DWI a modified SE sequence, *pulsed gradient spin echo* (PGSE) sequence is used.

2.4.1 Spin Echo Sequence

SE sequence uses two RF pulses: 90° pulse and 180° pulse. The 90° pulse is used to excite the system. It converts the magnetization vector *M* into xy-plane, like presented in Figure 2. The transverse magnetization M_{xy} starts immediately decay because the spins start to get out of phase. Next the second 180° pulse is applied. It will invert the spins and they start to move back into phase coherence. The time between the beginning of 90° pulse and the phase coherence is called *time of echo* (TE). In addition, the time between the new RF pulse sequence is called the *time of repetition* (TR). During the TR interval, T_2 decay and T_1 recovery occur in tissues. TR value range from extremely short (millisecond) to extremely long (tens of seconds). [2]

2.4.2 Gradient Echo Sequence

GE sequence uses only a single RF pulse, a 90° pulse. After the 90° pulse the spins start to diphase and simultaneously the magnetic field gradient is applied. After time TE/2, the reversal gradient is applied causing the rephrase of spins. This produces the *gradient echo*. [2]

2.4.3 Pulsed Gradient Spin Echo Sequence

In the case of diffusion weighted imaging, the often used imaging sequence is called *pulsed gradient spin echo* (PGSE), sometimes called *Stejskal and Tanner method* after its inventors. It is similar to SE sequence but two additional gradient pulses are applied symmetrically around 180° pulse. After the 90° RF pulse the first gradient lobe is applied and as a consequence the spins evolve freely. Statistic spins stand still while the moving spins change their relative position. Like in SE sequence, a 180° pulse is activated to refocus the spins. Finally, a second gradient lobe, of the same intensity as the first one, is applied. Static spins now remain the same situation as before the sequence. The moving spins instead do not recover the phase after the second gradient pulse because they have changed their position between both gradient lobes. The contrast in diffusion images arises from the fact that the signal from the average moving spins is lower than the one form the static spins. Schematic presentation of PGSE sequence is presented in Figure 4. [3; 9]

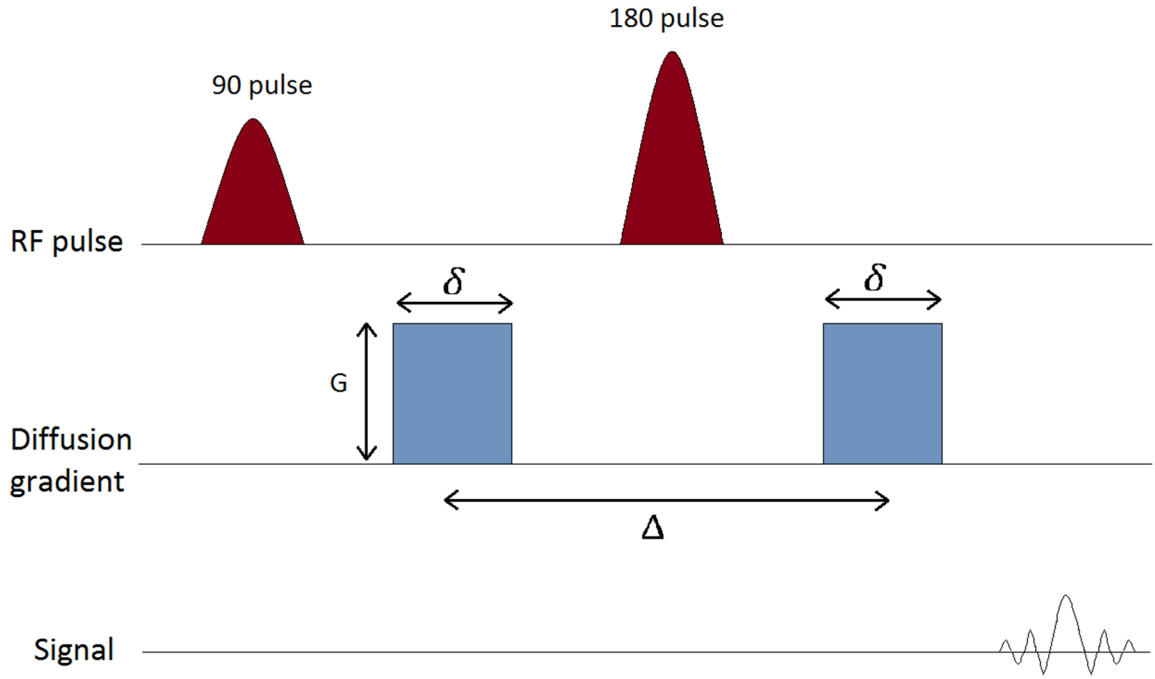

Figure 4. Schematic presentation of PGSE sequence. Two identical diffusion gradient pulses are inserted before and after a 180° pulse. Factors defining the degree of diffusion are the gradient amplitude G, duration δ, and the time between the two gradients Δ. Figure modified from [7].

2.5 Diffusion

Diffusion is a phenomenon in which molecules over *0 K* temperature experiment a Brownian motion caused by thermal energy and in consequence molecules from a region of higher concentration will move to a region of lower concentration. Diffusion can be modelled from a molecule point of view with *random walk* model, which considers movement of a single molecule and generalizes it into experimentally measurable variables, like diffusion constant. Another approach is to study diffusion from concentration gradient point of view with *Fick's law*.

2.5.1 Random walk

Brownian motion of a single particle can be modelled with *random walk*. In this model particle takes N steps of length L to random directions. The mean displacement r of a random walk is zero, but the square of the displacement has a nonzero average r^2, which is:

$$< (r)^2 > = NL^2. \tag{4}$$

If the particle takes a step in every time interval Δt, after total time t the particle has taken $N = t/\Delta t$ random steps. When defining the diffusion constant as:

$$D = L^2/(2\Delta t) \tag{5}$$

the mean-square displacement in a random walk becomes:

$$< (r)^2 \geq 2Dt, \tag{6}$$

which is also called the *diffusion law*. Diffusion constant *D* describes the intensity of the diffusion. From equation (6) can be seen that the mean-square displacement increases with time and with higher diffusion constant. So if molecules are let move longer time they will move further and if diffusion is strong molecules will also move further.

Diffusion is an event of random fluctuations. Random collisions also give rise to friction, which in case of fluids can be described with viscous friction coefficient ζ. For a spherical object the viscous friction coefficient is expressed with *Stokes formula*:

$$\zeta = 6\pi\eta R, \tag{7}$$

where η is the viscosity of the fluid and *R* is the radius of the particle. Einstein connected friction with diffusion with following formula:

$$\zeta D = k_B T, \tag{8}$$

where k_B is Boltzmann constant, *T* is temperature and ζ is the viscous friction coefficient. This *Einstein relation* shows that diffusion depends also on temperature and size of the particles; diffusion is greater in higher temperatures but high viscosity or big particles decrease diffusion. [12]

2.5.2 Fick's law

Random walk is a practical and simple model for diffusion of individual particles but when considering diffusion of larger amount of particles, like ink molecules in a glass of water, something more universal is needed to describe the diffusion process. One way is to study concentration profiles. Concentration differences create particle flux, which can be described with Fick's law (in one dimension):

$$j = -D\frac{dc}{dx}, \tag{9}$$

where *j* is the particle flux and *c* is the concentration. The intensity of flux describes the diffusion, thus the diffusion is greater with higher concentration gradient. [12] When considering the continuity equation *dc/dt = - dj/dx*, equation (9) can be further developed to the diffusion equation:

$$\frac{dc}{dt} = D\frac{d^2c}{dx^2}. \quad (10)$$

2.5.3 Diffusion types

Diffusion can be divided into three main types: *free*, *isotropic* and *anisotropic diffusion*. Free diffusion means movement of water molecules in environment with no obstacles. For example molecules in glass of water will diffuse freely through Brownian motion. [12; 13] Instead in isotopic diffusion the average distance of displacement of water molecules is the same in all directions. The difference to free diffusion is in the slight restriction of displacement due to for example cell membranes. Diffusion in biological tissues can often be considered as isotropic. [1; 13] In the case of anisotropic diffusion the movement of molecules is restricted in only certain spatial directions. For example in brain structures water molecules diffuse faster in the direction of axons than perpendicular to the axons. [1] Schematic presentation of different types is presented in Figure 5.

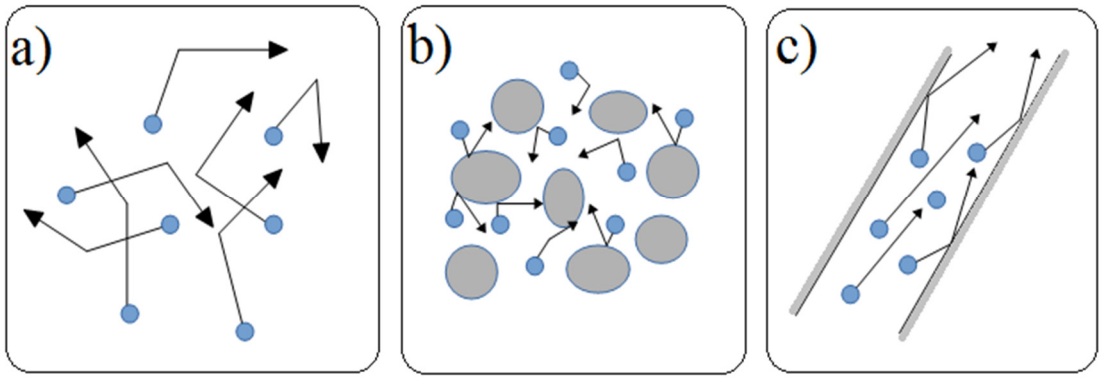

Figure 5. Schematic presentation of different diffusion types, modified from [13]. a) Free diffusion allows molecules to diffuse freely in all directions. b) In isotropic diffusion e.g. cells restrict diffusion but it is allowed in all directions. c) Anisotropic diffusion restricts movement in certain directions.

2.6 Diffusion-Weighted MRI

Diffusion-Weighted MRI (or *diffusion-weighted imaging*, DWI) is a medical imaging technique based on motion of water molecules. The MRI sequence sensitive to Brownian motion was introduced by Stejskal and Tanner already in 1965. [3] This sequence is described in *chapter 2.4.3*.

The DW images are produced by sensitizing the system with gradient pulses from different directions. The gradient strength can be described with *b-values*. With DW images obtained with multiple b-values from three orthogonal direction it is possible to produce *ADC maps*, which describe the *strength* of diffusion in tissues. However, to obtain information about the *direction* of diffusion, at least six diffusion gradient di-

rections are needed. This kind of direction diffusion imaging is called *diffusion tensor imaging* (DTI). [14; 15]

2.6.1 b-value

A *b-value* is a constant describing the gradient strength or the diffusion weighting achieved. It quantifies the amount of signal loss to be expected with a given pulse sequence for a given diffusion constant. [1; 16] b-value is proportional to the square of the gradient strength *G* in the following matter:

$$b = \gamma^2 G^2 \delta^2 (\Delta - \frac{\delta}{3}), \tag{11}$$

where γ is the gyromagnetic constant, δ represents gradient pulse duration, and Δ represents the separation between applied gradient lobes. Thus b value has units of s/mm^2. [3; 9]

2.6.2 ADC maps

The diffusion constant can be measured by performing multiple MRI scannings with different b-values. At least two different b-values are needed, but the accuracy may be improved through a greater number of b-values. The obtained diffusion constants are called as *apparent diffusion coefficients* (ADC), to differentiate them from the constant of diffusion in pure water (equation 5). [1] ADC using two b-values is determined as follows:

$$ADC = \frac{\ln(S_0 / S_1)}{b_1 - b_0}, \tag{12}$$

where b_i stands for the b-values and corresponding S_i intensities on the diffusion-weighted image. Images whose gray-scale values represent the mean ADCs of the corresponding voxels are known as *ADC maps*. [17]

Diffusion weighting depends on the applied diffusion direction. To obtain isotropic image, three orthogonal diffusion direction are needed to combine an ADC map. This isotropic image represents the effect of the average water movement in an isotropic tissue independently of the diffusion directions applied. [3] The direction dependent DW method, DTI is described in next chapter.

DW images describe the actual diffusion in tissues while the ADC maps tell the difference between two DW images. If water molecules can move relatively freely in tissues, they show lower pixel intensity S_i in DV images. This is because water molecules can be considered to “move out of the pixel”. On the other hand in the ADC map the difference to the original situation is high, which implicates that the ADC pixel val-

ue is also high. And vice versa, for high DW image intensity, the ADC values are lower. [18] This reasoning is presented schematically in Figure 6.

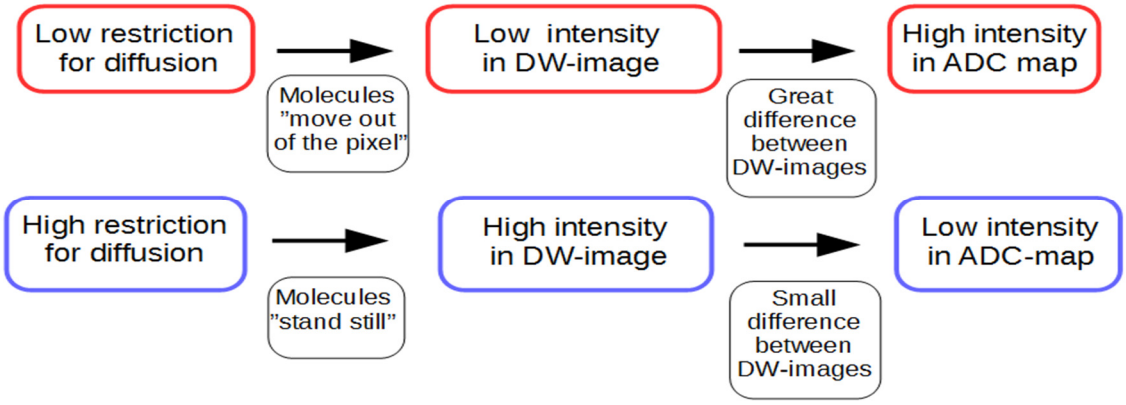

Figure 6. Relationship between molecule diffusion and image intensity in diffusion-weighted image and ADC map.

2.6.3 Diffusion Tensor Imaging

In anisotropic tissues the diffusion constant depends on the direction of applied diffusion gradients. A diffusion imaging where multiple directions are measured is known as *diffusion tensor imaging* (DTI). Now the diffusion properties of the tissues are described with a three-dimensional diffusion tensor $\overline{D}$:

$$\overline{D} = \begin{bmatrix} D_{xx} & D_{xy} & D_{xz} \\ D_{yx} & D_{yy} & D_{yz} \\ D_{zx} & D_{zy} & D_{zz} \end{bmatrix}, \tag{13}$$

where in each D_{ij} the first subscript refers to tissue orientation and the second refers to the gradient orientation. The diagonal elements D_{xx}, D_{yy} and D_{zz}, correspond to three orthogonal direction, which are used also in determination of scalar ADC values. [9; 19]

Diffusion tensor $\overline{D}$ as such is not ideal form to visualize the diffusion. Further processed way is to visualize diffusion with scalar parametric maps, like mean diffusivity (MD) and fractional anisotropy (FA). [14] MD presents the strength of diffusion by means of eigenvalues λ_1, λ_2, and λ_3:

$$MD = \frac{\lambda_1 + \lambda_2 + \lambda_3}{3}. \tag{14}$$

FA instead shows the degree of anisotropy in tissues. It is described with following formula:

$$FA = \sqrt{\frac{3}{2}} \frac{\sqrt{(\lambda_1 - MD)^2 + (\lambda_2 - MD)^2 + (\lambda_3 - MD)^2}}{\sqrt{\lambda_1^2 + \lambda_2^2 + \lambda_3^2}}, \quad (15)$$

where λ_i is the eigenvalue and MD the mean diffusivity (equation 14). The values of FA range from 0 (completely isotropic) to 1 (completely anisotropic). [3]

2.6.4 Potential clinical applications of DWI

DWI has potential applications especially in oncology, because tumor tissues have different cellularity compared to normal tissue. Cancerous tissues restrict water diffusion of water molecules more than normal tissues and thus have lower ADC values than normal tissue. Different review articles [17; 20] suggest that DWI could be used for example in tumor detection, tumor characterization, monitoring treatment response, and predicting treatment response. Possible application targets could be for instance liver, pancreas, kidney, breast and prostate cancers. Even whole body diffusion imaging is studied. However, its main limitation are the sensitivity to motion influences, like cardiac and respiratory movements. [3; 17]

The directionality information of DTI can be best utilized in studying brain tissues. For example cerebral ischemia, epilepsy or brain tumors can be diagnosed with DTI. In many brain disorders the early diagnosis is crucial and DTI has great advantage in information from cellular level when compared to traditional imaging methods like CT and MRI. [9; 21]

3. BREAST CANCER

Breast cancer is the most common cancer type among women. Only lung cancer causes more cancer-related deaths in women. Breast cancer has become more and more frequent during last decades: in Finland in 2011 there were 4865 new cases. Breast cancer frequency increases substantially among the women after the age of 45 and the average age for diagnosis is at the age of 60. Breast cancer is diagnosed also for the women under the age of 30 but in this age group it is rare. [6]

3.1 Normal Breast

In humans, paired mammary glands rest on the pectoralis muscle on the upper chest wall. The female breast consists mainly of lobules, ducts and stroma. Stroma is connective tissue that surrounds the ducts and lobules. [4; 22] There are usually six to ten major ducts which branch further into smaller ones. Eventually the terminal duct branches into a grapelike cluster of small acini to form a lobule. Lobules are the milk producing glands that are modified sweat glands. (Fig. 7) [22-24]

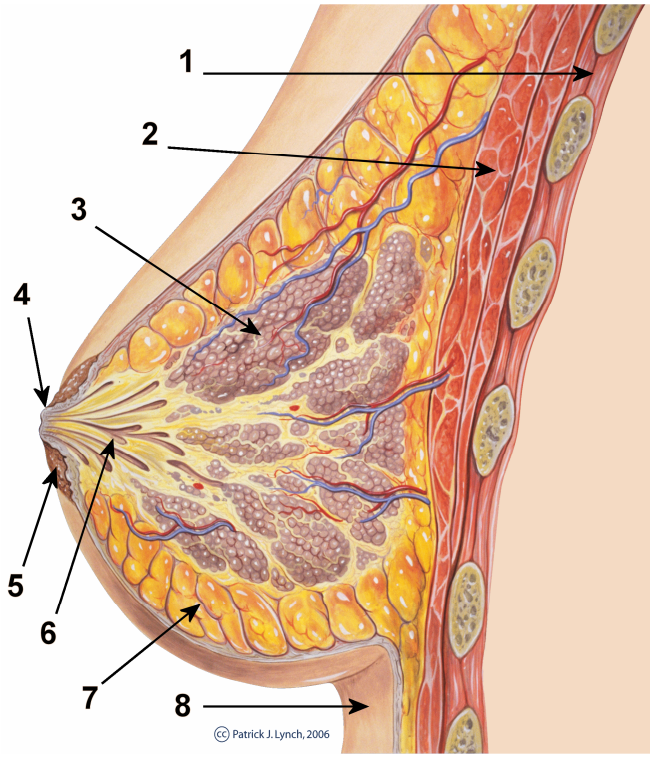

Figure 7. Female breast structure, "*Breast anatomy normal scheme*" by Original author: Patrick J. Lynch. The arrows show 1. chest wall, 2. pectoralis muscles 3. lobules 4. nipple 5. areola 6. milk duct 7. fatty tissue and 8. skin. [25]

3.2 Breast tissue changes

Breast tissue changes, or breast lesions can be divided into two groups: *benign* and *malign* lesions. Malign lesions, or *cancerous tumours*, are fast-growing lesions. They can grow invasively into the surrounding tissues or spread to other parts of the body, which is called *metastasis*. Malign tumours are often fatal because of the invasive nature and the ability to form metastases. [5]

Benign lesions instead are not cancerous. They are typically slow-growing and can be well distinguished from the surrounding tissue. Benign lesions do not invade into other tissues and they do not form metastases. Benign lesion cells resemble the normal tissue cells both in structure and in functional features. Usually benign tumours are not life threatening. Separation between malignant and benign tumors is made through a histo-pathological study. [4; 5]

3.2.1 Benign Lesions

The majority of breast abnormalities are benign. They can be classified into three groups according to later risk of developing breast cancer: *Nonproliferative breast changes*, *proliferative breast changes* and *atypical hyperplasia*. Only certain way to distinguish benign lesions from malignancy is biopsy and histologic examinations. [23; 24; 26]

Nonproliferative breast changes

Nonproliferative changes (also *called fibrocystic changes*) are not associated with a risk of breast cancer. They are most common group of disorders of the breast for women between ages 20 and 40 [23; 24]. Typical histological features of fibrocystic changes include for example *cysts*, *expansion of lobules*, and *stromal fibrosis*. The cause of these changes is not clear and it is thought to be related to a localized imbalance between estrogen and progesterone. [23]

Proliferative breast changes and atypical hyperplasia

Proliferative changes are associated with small increase in the risk of later carcinoma. Lesions are characterized with proliferation of epithelial cells but they are not clonal and are not commonly found to have genetic changes. There are different types of proliferative changes, e.g**.** *epithelial hyperplasia*, *sclerosing adenosis*, and *papilloma*. [24]

Atypical hyperplasia is associated with increased risk of carcinoma. It includes two forms: *atypical ductal hyperplasia* and *atypical lobular hyperplasia*. These atypical hyperplasia have histologic resemblance to *carcinoma in situ* (described later). [24]

3.2.2 Malignant lesions

There are several types of breast cancer, which can be divided into two main groups: *in situ carcinomas* and *invasive carcinomas*. In the case of carcinoma in situ the tumor has

limited to ducts and lobules by the basement membrane. Invasive carcinoma instead has penetrated through the basement membrane into the stroma. These two main groups divide into numerous sub types. In this chapter the most common types are introduced. [24]

Carcinoma in situ

Carcinoma in situ can also be called as *non-invasive* or *pre-invasive* carcinoma due to its possibility to develop into invasive carcinoma if left untreated [4; 26]. There are two types of in situ carcinomas: *ductal carcinoma in situ* and *lobular carcinoma in situ*. These both types usually arise from cells in the terminal duct lobular unit. [26]

Ductal carcinoma in situ

Ductal carcinoma in situ (DCIS) is an intraductal lesion limited to ducts and lobules with no evidence of invasions through basement membrane into surrounding stroma. Hence, DCSI can be considered a pre-cancer because some cases can develop and become invasive carcinoma. [4; 23; 24] Due to mammographic screening, the DCIS cases are found more easily. Nowadays 15-30 % of all breast carcinomas are diagnosed as DCIS in Finland whereas before the screening the portion was only 5 %. [5]

Lobular carcinoma in situ

Lobular carcinoma in situ (LCIS) can be considered as preliminary stage for invasive lobular carcinoma as the cells of LCIS are identical with the cells of invasive carcinoma and they share genetic abnormalities [24]. Cancerous cells fill the lumen of lobules and LCIS usually expands but does not alter the acini of lobules [5; 26]. LCIS lesions cannot be found with mammography since they are not associated with calcifications or stromal reactions that produce mammographic densities [24]. Therefore LCIS if pretty rare: in Finland only 1-6% of all breast cancers are diagnosed as LCIS. Approximately 25% of patients diagnosed with LCIS will develop invasive carcinoma in 25 years. [5]

Invasive carcinoma

An invasive cancer is carcinoma that has already grown beyond the basement membrane. Most breast cancers are invasive carcinomas. Here the most common ones, invasive ductal carcinoma and invasive lobular carcinoma, are presented. [4; 24]

Invasive ductal carcinoma

Invasive ductal carcinoma (IDC) is the most common type of breast cancer: in Finland 70 % of the breast cancers are IDC [4; 6]. This type of cancer is often associated with DCIS and rarely with LCIS. [26] IDC begins like DCIS but breaks through the basement membrane and grows into the stroma. It produces a desmoplastic response, which replaces normal breast fat and forms a hard, palpable mass [26]. IDC can also metastasize to other parts of the body through the lymphatic system. [4]

Invasive lobular carcinoma
Invasive lobular carcinoma (ILC) is second common breast cancer type in Finland: 10-20% of all breast carcinoma cases [6]. In the case of ILC, cancerous cells invade individually into stroma and are often aligned in "single-file" strands or chains. This is why ILC may be harder to detect by a mammogram than IDC. [4; 26] Like IDC, lobular carcinomas can also metastasize to other parts of the body; they more frequently spread to cerebrospinal fluid, serosal surfaces, gastrointestinal tract, ovary, uterus, and bone marrow. Lobular carcinomas also are more frequently multi-centric and bilateral. [4; 26]

3.3 Breast Cancer Imaging Methods

Breast imaging is needed in different breast imaging areas, for example in screening for breast cancer and classifying breast abnormalities. In this chapter the common breast imaging method are presented briefly and discussed when and why they are used in breast imaging. After this new potential breast imaging method, diffusion-weighted imaging, is introduced and its contribution is estimated. Eventually different methods are compared.

3.3.1 Mammography

Mammography is the most used technique for breast cancer detection. It is a low-dose x-ray system designed especially for imaging breasts. [27] In mammography imaging the breast is compressed with plastic plate to obtain better quality images. Images are taken usually from at least two direction: craniocaudal and mediolateral projections [28]. Mammography is used both in screening and diagnosis of breast cancer. [29]

The screening mammography is performed among asymptomatic women without a personal history of breast cancer. [29] In Finland women of ages 50-69 are screened every second years [30]. Goal of the mammographic screening is to find breast carcinomas as early as possible, before they cause any symptoms or palpable masses. [28; 29] Tumors found with screening are usually less than 1 cm in diameter [28]. The size of a tumor and how far it has spread are important factors in predicting the prognosis for a patient. [4] If an abnormality is found in screening mammography, additional imaging is needed. This can be done with diagnostic mammography. Imaging direction vary according to each study. [29]

3.3.2 Ultrasound

Ultrasound (US) is widely used breast examination method, which applies ultrasound waves and acoustic properties of the body to produce medical images. [28] Ultrasound represents the sound waves with frequency above 20 kHz. Medical ultrasound uses frequencies starting from 2 MHz up to 20 MHz, with special ultrasound applications up to

50 MHz. Ultrasound is produced and detected with a *transducer*. It converts the electrical energy into mechanical energy to produce ultrasound and mechanical energy back to electrical energy for ultrasound detection. [2]

In breast cancer examination US is operated along with mammography. It is usually used as further study for mammographic finding, for example to distinguish cysts and solid masses. [4; 28] Moreover, US can be used to image palpable mass in dense breast tissue. Especially among young women the breast tissue is dense and thus contrast in mammography might be poor. [28]

3.3.3 Magnetic Resonance Imaging

MRI technique is discussed in detail in the *Chapter 2*. In breast cancer examination contrast-enhanced MRI (DCE-MRI) is used, like US, in further studies for masses found in mammography. It is also used for screening of women at high risk for development of breast cancer. [4; 6] According to *American Cancer Society*, this includes women who have a known *BRCA1* or *BRCA2* gene mutation or who have first-degree relative with these gene mutations but are themselves untested. Annual screening is also recommended for women with 20-25% or greater lifetime risk of cancer development based on family history and for women who have received radiation therapy to the chest between ages of 10 and 30. Furthermore, women with *Li-Fraumeni syndrome*, *Cowden syndrome*, or *Bannayan-Riley-Ruvalcaba syndrome*, or first-degree relatives with one of these syndromes are recommended to have MRI screening in addition to mammographic examination. [4]

3.3.4 Diffusion-Weighted Imaging

Diffusion weighted imaging (DWI) is a MRI technique that measures the mobility of water molecules, described in detail in c*hapter 2.6*. The contrast in DWI arises from the changes of water mobility in different tissues. Since the tissue properties differ between benign and malign lesions, DWI imaging can be used for lesions type differentiation. [31; 32]

Tissue properties and ADC values

The degree of motion measured by DWI relates to the *mean path length* travelled by water molecules in the tissue within specific observation time period. In biological tissues the motion is restricted by intracellular and extracellular compartments, and macromolecules. In tissues with low cell density the mean path length travelled by water molecules is much greater than in tissues with high cell density (Figure 8). Thus the degree of water diffusion in biological tissues is inversely correlated with the tissue cellularity. [7; 33]

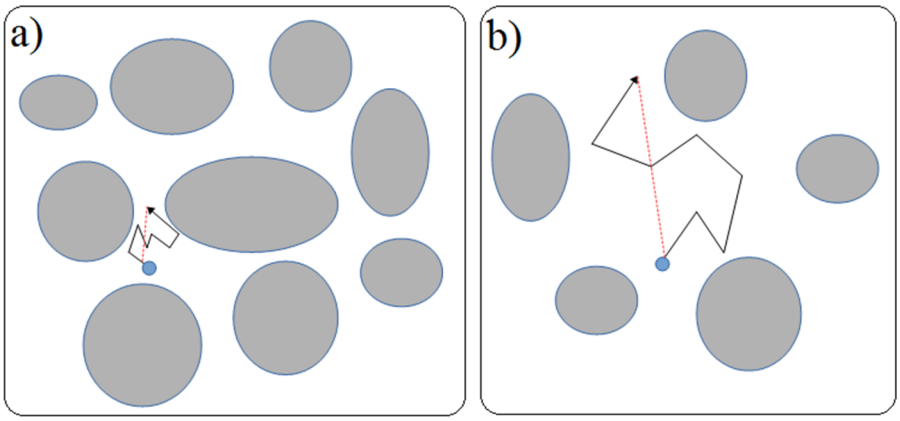

Figure 8. Schematic presentation of how the cellularity of tissue affects the distance traveled by water molecules in extracellular space. a) In high cellularity tissue the mean path length (red line) travelled by water molecules is shorter than in b) low cellularity tissue. So the degree of water diffusion in biological tissues is inversely correlated with the tissue cellularity. Figure modified from [7].

Breast tumors typically have high cellular density, thus the diffusion of water molecules is more restricted in malignant tissue than in benign lesions or normal breast tissue. Like described earlier in *chapter 2.5.2*, restricted diffusion indicates high signal intensity on diffusion-weighted images and further low ADC values. By contrast, benign lesions usually exhibit low intensities in DW images and higher ADC values. However, the differentiation is not so straight forward due to overlapping of malign and benign lesion ADC values. For example DW imaging of DCIS is controversial: Depending on whether DCIS appears mass-forming or low cellularity form its DW image intensity differs. Consequently, most of the false-negative cases reported at DWI of breast represents DCIS. [7; 18] In addition, in the case of benign changes the signal intensity may be influenced by used b-value [18]. ADC values for benign and malign lesions can be found widely in literature. The ADC values for normal breast tissue are about *1.51-1.91 x10^{-3} mm^2/s* for b-values 0 and 1000 s/mm^2 [34; 35]. Summary of measurement results from different studies are combined into Table 1.

Table 1. ADC values of benign and malign lesions from various studies. [34-43]

Study	b-values (s/mm^2)	Benign		Malign	
		ADC (10^{-3} mm^2/s)	N	ADC (10^{-3} mm^2/s)	N
Abdulgraffar et al. (2013)	59, 400 and 800	1.48 ± 0.33	22	0.93 ± 0.27	21
Bogner et al. (2009)	50 and 850	1.47 ± 0.21	17	0.99 ± 0.18	24
Gouhar et al. (2011)	0 and 1000	1.46 ± 0.48	51	0.92 ± 0.23	27
Guo et al. (2002)	0, 250, 500, 750 and 1000	1.57 ± 0.23	24	0.97 ± 0.20	31
Kuroki et al. (2004)	0 and 1000	1.448 ± 0.453	5	1.021 ± 0.23	55
Marini et el. (2007)	0 and 1000	1.48 ± 0.37	21	0.95 ± 0.18	42
Moukhtar et al. (2014)	0 and 750	1.34 ± 0.36	23	1.02 ± 0.30	48
Park et al. (2007)	0 and 1000	1.41 ± 0.56	4	0.89 ± 0.18	43
Spick et al. (2014)	50, 400 and 800	1.53 ± 0.38	84	1.06 ± 0.27	20
Woodhams et al. (2005)	0 and 750	1.67 ± 0.54	24	1.22 ± 0.31	167

Imaging protocol optimization

ADC values of lesions depend on used b-values. With low b-values the diffusion weighting effect is weaker and thus also perfusion effects are strongly present in DW images. Instead at higher b-values, the diffusion effects are stronger than perfusion so DW images are mainly based on diffusion effects, like can be seen in Figure 9. ADC values are larger with low b-values and vice versa. Because of this the measured ADC values are comparable only with studies acquired with same b-values. [44]

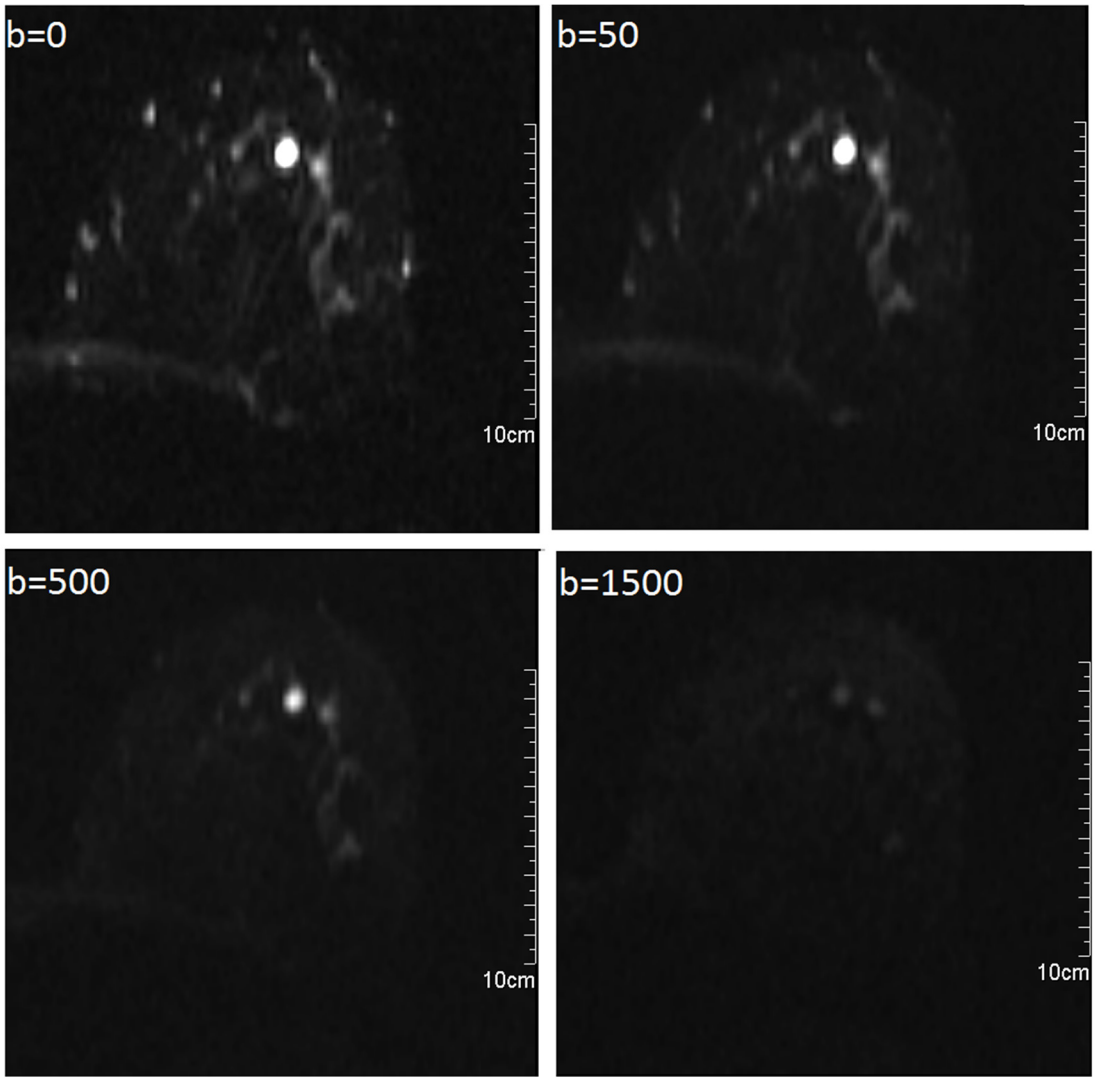

Figure 9. Effect of different b-values (unit *s/mm*^{2}) to DW images. In low b value images the veins can be seen clearly due to perfusion. Instead in high b value images the diffusion effects are stronger.

The choice of b-values depends on the imaging application. In breast imaging the optimal b-values should give good contrast for lesions and normal breast tissue. To minimize the perfusion effects higher b-values are favored but on the other hand they also decrease the signal-to-noise ratio. Many studies [7; 18; 35; 45] indicate that b-values between *800-1500 s/mm*^{2} give best contrast. Like discussed in *chapter 2.6.2* the accuracy of ADC map may be improved with the use of multiple b-values. However, studies of multiple b-values [44; 46] found no improvement over two b-value acquisitions. Thus in clinical practiced DW imaging with two b-values is reasonable for time saving.

Diffusion-weighted imaging of breasts is technically challenging for several reason: tissue-air interfaces at skin surface and at thorax give rise to susceptibility artefacts and high fat tissue content causes image artefacts such as ghosting and chemical shift. The optimal *fat suppression* technique and good *shimming* are therefore essential

for high-quality DW imaging of the breast. Shimming is used to decrease magnetic field inhomogeneities. Improved shimming, or a higher magnetic field strength, allows better spectral separation of water and fat resonances, and thus better fat suppression. [7; 18]

Contrast between tumor and normal breast tissue in ADC-maps may not be as significant without appropriate fat suppression. There are two common ways for fat suppression in breast DWI: *spectral fat suppression* and *inversion recovery*. They both have their advantages and disadvantages but in general spectral fat suppression is preferred [7]. In addition to different technical tasks patient positioning is crucial for image quality. For example skin folds may cause inhomogeneous fat suppression. Also cosy position avoids unnecessary moving of patient during imaging. Patient motion between different diffusion-gradient images causes misregistration and further errors in ADC calculations. [7; 18] The imaging parameters for optimal imaging discussed above are combined in Table 2. Also some other parameters are listed based on articles of *R. Woodhams et al.* [18] and *S.C. Partidge and E.S. McDonald* [7].

Table 2. Imaging parameters for example diffusion-weighted imaging protocol. [7; 18]

Parameter	**Specification**
Imaging sequence	Spin-echo echo-planar imaging
b-value	0, 800-1000 s/mm2
Fat suppression	Spectral fat suppression
Slice thickness	4-5 mm
Imaging time	4-6 min

3.3.5 Comparison of Imaging Methods

Mammography can be considered as the conventional breast imaging method at the moment. Because of this, it is widely available and also cheap imaging method. [4; 6] Even relatively small lesions are visible in mammography but its sensitivity varies widely (35-95 %) depending the structure of breast tissue [6]. Poorest sensitivity occurs with young women whose breast tissue is often dense and contains only little fat. Dense breast tissue is a major limitation of mammography. [6; 47]

Ultrasound is cheap, nonionizing, and widely available imaging method. [4] Breast imaging study by *Kolb et al.* [48] compared the sensitivity of mammography to US with different density categories. With highest density level the sensitivity of mammography was found 47.8% and of US 76.1%. Also other studies combined in review article [47] by *P. K. Ravert et al.* show an increase in the diagnostics of breast cancer by US in women with dense breast. However, US is not accurate method to detect small lesions (less than 1 cm in diameter). Thus it is not suitable for screening method of breast cancer but important as an additional method for mammography. [4; 28] New

ultrasound devices are capable of measuring lesions as small as 1-2 mm in diameter, which makes US important additional imaging method for mammography [27].

MRI provides sensitive imaging with high accuracy, especially DCE-MRI technique. Its sensitivity and specificity are far better than with mammography and US, sensitivity even 70-90% with young women [6]. However, it also has a higher false-positive rate and its usability is limited in the detection of calcifications. Moreover, the disadvantages of MRI compared to mammography and US are the long scan times, usually 20 to 30 min, and the need for contrast medium. In addition, the contrast material increases the cost and is not suitable for all. Also claustrophobic persons are not comfortable with MR imaging. [4; 6; 29; 43]

Like discussed in previous chapter DW-MRI has potential for improve the sensitivity of traditional MRI. Thus false-positive rates could be reduced and unnecessary biopsies avoided. The contrast imaging without added contrast material is better for patients and also cheaper and faster. However, more research is needed before wide clinical use. [7; 18] The advantages and disadvantages of different methods are collected into Table 3. Also future prospects of the methods are estimated.

Table 3. Advantages and disadvantages of different breast imaging methods combined: mammography (MG), ultrasound (US), magnetic-resonance imaging (MRI) and diffusion-weighted magnetic resonance imaging (DW-MRI).

Method	Pros	Cons	Future
MG	○ cheap ○ widely available ○ long traditions in breast imaging	○ low sensitivity with dense breast	○ stays as prime breast imaging method
US	○ cheap ○ widely available ○ nonionizing	○ not accurate for small lesions	○ Additional method for mammography
MRI	○ good resolution ○ high sensitivity ○ high specificity ○ nonionizing	○ expensive ○ time consuming ○ not suitable for claustrophobic persons	○ additional imaging for mammography ○ screening for women with high breast cancer risk
DW-MRI	○ cheaper and faster than DCE-MRI ○ more sensitive than DCE-MRI ○ nonionizing	○ more research needed before clinical use ○ availability	○ Instead of DCE-MRI

4. MATERIALS AND METHODS

Materials used in this project were imaged in *Turku University Hospital* with *Siemens Avanto 1.5 T* device. Four different studies were carried out using DW image and contrast-enhanced MR image (DCE-image) series: Comparison of mean ADC values of benign and malign lesions, repeatability of ADC measurements, correlation between SNR and ADC values, and effect of lesion size to ADC values. In this chapter the used data and imaging parameters are introduced. Moreover, the steps used in measurement, calculations, and statistical analysis with *SPSS software* are explained.

4.1 Subjects

Data of the study included originally MR images of 50 patients collected in *Turku University Hospital* during February 2011 and February 2013 by doctors *Ilkka Koskivuo* and *Nina Brück*. From these two patients were excluded due to different imaging device and three patients due to failed fat suppression on the images. Therefore the research was performed for 45 patients with age differing between *45* and *83* years, with average age of *60* years. Patients had altogether *48* malignant lesions, *5* malign suspects and *8* benign lesions. All the carcinomas were ductal carcinoma in situ. Data characteristics are gathered into Table 4.

Table 4. Details of data.

Lesion type	**Number of lesions**	**Area range** (cm^2)	**Mean area** (cm^2)
Malign	48	0.14 - 1.53	0.56
Malign suspect	5	0.17 - 0.46	0.29
Benign	8	0.14 - 0.57	0.34

4.2 MRI acquisition

Siemens Avanto 1.5 T device was used for imaging. MRI was performed using *T2-weighted*, *DWI*, and *T1-weighted* imaging sequences. *T2-weighted imaging* was done with imaging parameters of: 39 slices with a field of view (FoV) 360 mm, a slice thickness of 3.0 mm and voxel size 0.9x0.7x3.0 mm. SPAIR fat-suppressed *DW imaging* was performed with b-values of 0, 50, 500 and 1500 s/mm^2 with 3 diffusion directions. Other parameters were: 30 slices with a FOV of 360 mm, a slice thickness of 5.0 mm and

voxel size 2.4x1.9x5.0 mm. *T1-weighted* contrast-enhanced imaging sequence was performed after DWI sequence with following parameters: slice thickness 1.00 mm, FoV 360 mm and voxel size 1.1x0.8x1.0 mm.

4.3 ADC measurements

Two different ADC measurements were performed: Measurement of ADC values of benign and malign lesions, and repeatability measurements. First step in the studies was to measure ADC values from the ADC maps with *SyngoMMWP VE 36A* –program. After this the needed calculations were performed to obtain wanted results.

4.3.1 Benign and malign lesions

Diffusion values for benign and malign lesions were measured by selecting the *region of interest* (ROI) in ADC map. The measurement were done by MP with no previous experiment from medical image viewing. The measurement procedure was as follows:

1. Lesion as localised in contrast-enhanced MR image (DCE-image). Its coordinates and size were measured with image program tools.
2. The corresponding lesion location was searched in ADC map with the help of the obtained coordinates and ROI as drawn with the circular drawing tool. It as important to include a homogenous area inside the circle, i.e. exclude all boundaries and other dissimilar areas. The size of the ROI was maximized but yet limited to the size measured in DCE-image. Values of mean, standard deviation and area were wrote down.
3. In order to be able to compare results between patients, it was necessary to normalize the results. For this reason, background noise and two reference points from surrounding tissue were measured.
    I. First reference point was drawn with circular tool into high intensity area. The size of this ROI is 1 cm^2.
    II. The second reference point as drawn into homogenous tissue. Homogeneity could also be verified in DCE-image. Often these kind of areas had low intensity. This ROI was also 1 cm^2 in size.
    III. Noise level was determined from background of the image, i.e. outside the patient. This ROI as drawn as 10 cm^2.

    Reference point are drawn closest to 2-3 cm to the actual lesion. Reference points can be also measured from the other breast or from other slice than the actual lesion.

Often lesion could be clearly seen also in the ADC image but sometime, especially with small lesions, the coordinates obtained from DCE-MR images were used as guidance. An example of ADC measurement is shown in Figure 10.

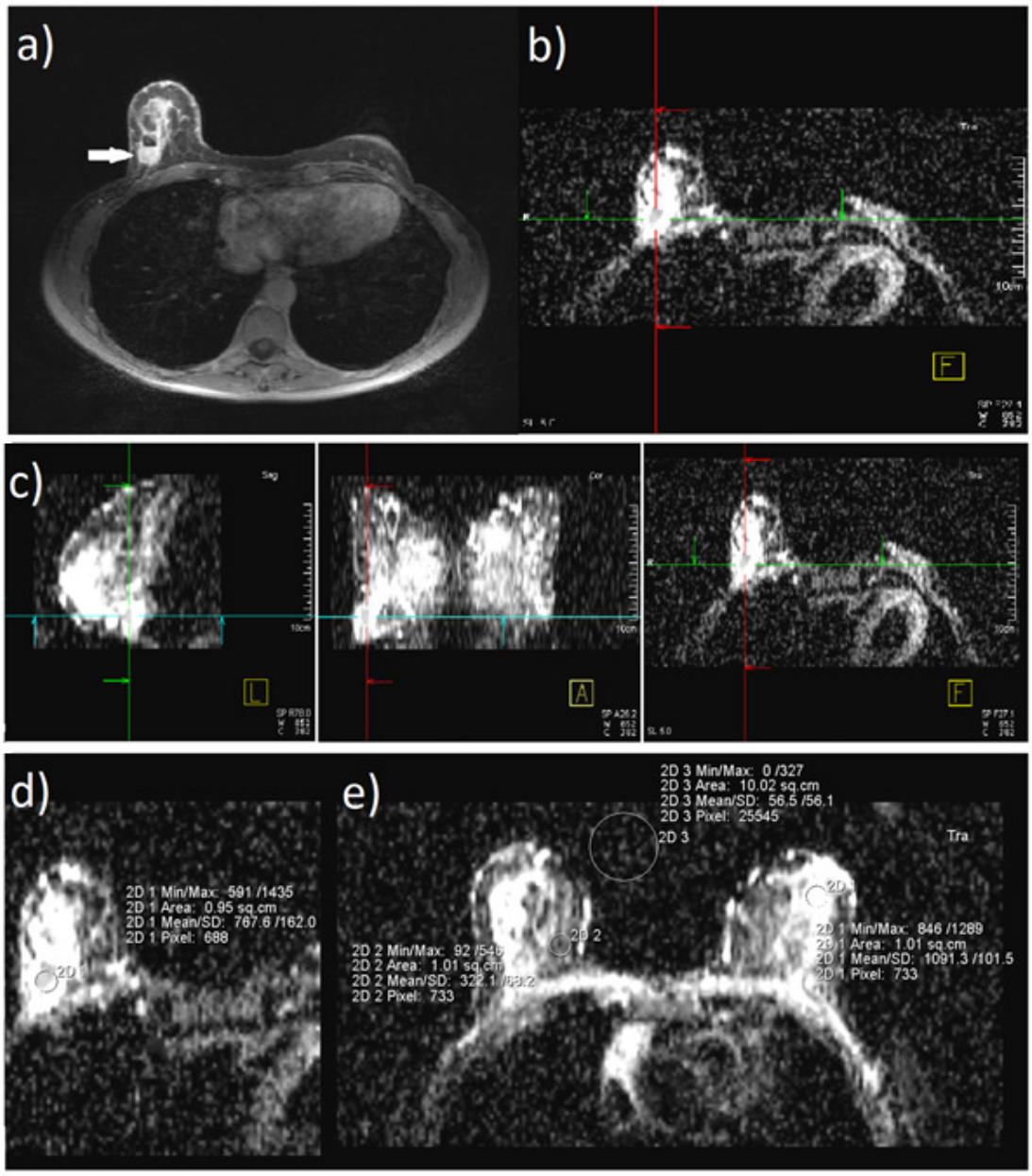

Figure 10. Example of ADC measurement. a) First lesions was localized in DCE-MR image (now shown with white arrow) and b) with the help of obtained coordinates its corresponding location was searched in ADC maps. c) ADC map could be visualized from three directions, *sagittal, coronal and transverse*. d) The ROI was drawn carefully into the lesion. e) Three reference ROIs were drawn into high intensity area, homogenous tissue area and into the background (outside the patient).

4.3.2 Repeatability

The reliability of ADC measurements was tested with repeated measurements. The measurements were performed for 16 randomly chosen malign lesions by same measurer (MP) seven month later than first ADC measurements. Measurements were performed like described in previous chapter (4.3.1). The repeatability was evaluated through intra-class correlation (ICC) values.

4.4 Signal-to-Noise ratio and lesions size measurements

Signal-to-Noise ratio (SNR) and lesion size measurements were performed to study the correlation between them and ADC values.

4.4.1 Signal-to-Noise Ratio

When determining the noise levels of images, the diffusion values for lesions and background were measured from DW images. The DW images with $b=0\ s/mm^2$ were used for this measurement. Lesion position was searched in DW image. If necessary, DCE-MR image was used to check the location. Using circular tool, ROI was drawn inside the lesion. It was important to not include any boundary of the lesion or other inhomogeneous area inside ROI circle. Second ROI was drawn to background of the image, i.e. outside patient. Its size was fixed to approximately 7.5 cm^2. An example of noise level measurement is shown in Figure 11.

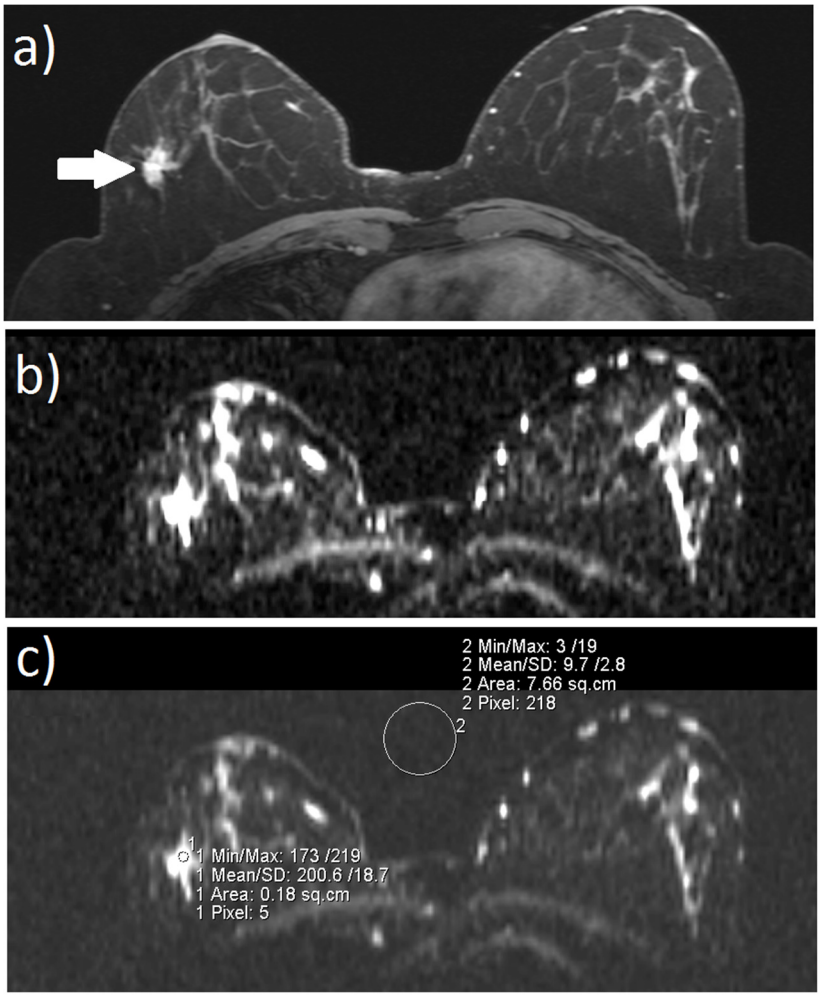

Figure 11. a) The white arrows shows the lesions in DCE-MR image. b) The b=0 s/mm^2 DW image. Lesions can be seen in left breast of the figure as bright spot. c) With circular tool ROI is drawn carefully inside the lesions and into the background, outside the patient.

4.4.2 Lesions size

The measurements of lesions size were performed by MP. The procedure was same as described in part 4.3.1. For this analysis size of only malign lesions were considered. Lesions were divided into three size groups: small, medium and large for further analysis.

4.5 Data Analysis Methods

The statistical significance of different measurements was tested with statistical tests using *SPSS Statistics 22 -software* (IBM, USA). Here the theories of the used tests are explained.

4.5.1 Normalization

ADC values of lesions were normalized with ADC value obtained from the reference point. Normalized ADC value ADC_n were determined with following calculation:

$$ADC_n = \frac{ADC_{lesion}}{ADC_{reference}}, \tag{16}$$

where ADC_{lesion} is the ADC value of actual lesion and $ADC_{reference}$ the mean ADC value from reference ROI. The more consistent results with literature values (Table 1) were achieved by using the reference point from high intensity area.

4.5.2 Signal-to-noise ratio

Signal-to-noise ratio was determined from *b=0* s/mm^2 diffusion images according the *NEMA Standards 1-2008*. SNR was obtained by dividing the image signal by the image noise:

$$SNR = \frac{signal}{noise}, \tag{17}$$

where *signal* is the mean signal measured from the lesion and *noise* is determined from the background of the image (outside of tissue area). The change of noise distribution must be modified because the SNR measure assumes the noise is Gaussian distributed. In this work the noise was corrected as:

$$noise = \frac{SD}{0.66}, \tag{18}$$

where SD is the standard deviation measured from the background and the factor of 0.66 ($\cong \sqrt{(4-\pi)/2}$) accounts for the Rayleigh distribution of the noise. The equation (17) was used to determine the SNR of the images. SNR was measured from 19 images and the final value was averaged from these.

4.5.3 Statistical methods

Before making any conclusions of statistical research results, they are usually being tested. This is often made through a *statistical hypothesis testing*. First a *null-hypothesis* H_0 is formed, which expresses the desired condition, e.g. "sample values are normally distributed". Also an *alternative hypothesis* H_1 is defined, which can be allowed if null-hypothesis is rejected, e.g. "sample values are not normally distributed". Next the statistical test is chosen to prove which hypothesis is correct. In this context also a *significance level* α for significant and nonsignificant statistics is defined. Common values for significance level are 5% and 1%.

Not always the hypothesis is selected correctly after the statistical test. Thus, two kinds of errors may occur; rejecting the null-hypothesis H_o when it is true or accepting it when it is false. These two errors are called as *Type I* and *Type II errors*, respectively. One way to avoid errors is to select appropriate significance level α. [49; 50]

Kolmogorov-Smirnov test

Kolmogorov-Smirnov test utilises cumulative distributions to compare experimental results with reference distributions [49]. In this work it was used to test if data samples were normally distributed. The null-hypothesis H_0 was set as "*The distribution of measured values is Gaussian*" and the alternative hypothesis H_1 as "*The distribution of measured values is not Gaussian*".

In Kolmogorov-Smirnov test the sample cumulative frequency sum $F_n(x)$ is determined for the data. This is then compared with cumulative distribution function of the reference distribution $F_e(x)$:

$$D = \left| F_n(x) - F_e(x) \right|, \tag{19}$$

where D is the difference. If the difference D does not exceed the appointed significance level α, the null-hypothesis is accepted. [50] In this thesis *Kolmogorov-Smirnov test* was used to test the normal distribution of samples.

t test

The tests for a difference between two means can be divided into two cases: samples large enough that the sample standard deviations are not practically different from known and the case of small-sample estimated standard deviations. The mean test uses a

standard normal distribution (*z distribution*) in the first case and a *t distribution* in the second one, and the tests are called *z test* and *t test*, respectively. [50]

Before the actual *t* test, the normality of the sample is tested (e.g. with Kolmogorov-Smirnov test). Then the null- and alternative hypotheses are specified. The null hypothesis H_0 is usually set as" *the means are the same*", $H_0: \mu_1 = \mu_2$. The alternative hypothesis H_1 "*the means are not the same*" may be set as two-sided test, $H_1: \mu_1 \neq \mu_2$ or as one-sided test, $H_1: \mu_1 < \mu_2$ or $H_1: \mu_1 > \mu_2$. By choosing the significance level, the critical *t* value can be determined from statistics tables. For the sample, the *t* value is calculated as:

$$t = \frac{\mu_1 - \mu_2}{s}, \tag{20}$$

where s is determined through following equation:

$$s = \sqrt{\left(\frac{1}{n_1} + \frac{1}{n_2}\right)\left[\frac{(n_1 - 1)s_1^2 + (n_2 - 1)s_2^2}{n_1 + n_2 - 2}\right]}, \tag{21}$$

where n_i is sample size and s_i is sample's standard deviation. Finally the null hypothesis is either accepted or rejected, depending on where the statistics lies relative to the critical value. [50] In this work *t test* was used to test if mean ADC values of benign and malign lesions were statistically significantly different.

The intra-class correlation

The intra-class correlation is a method for estimating the reliability of repeated measurements. The procedure is based upon the analysis of variance and the estimation of variance components. [51] It was introduced by Ronald Fisher [52]. The ICC values vary from 0 to 1 and the closer to unite they are, the more reliable the tested method is. The repeated measurements were analysed with SPSS using the averages of intra-class correlation coefficients (ICCs) with absolute agreements.

Sensitivity and Specificity

Sensitivity tells the proportion of true positive cases, so the event of a predicted disease being present. Specificity instead, also called true negative, is the event of predicting no disease when disease is absent. [50] In this thesis these concepts were used alongside with the ADC threshold values; for example threshold ADC value for malign lesions *X*. Sensitivity is determined with ratio:

$$sensitivity = \frac{Number\ of\ lesions\ with\ ADC\ value\ smaller\ than\ X}{Number\ of\ malign\ lesions} \tag{22}$$

Respectively the specificity is described with ratio:

$$specificity = \frac{Number\ of\ benign\ lesions\ with\ ADC\ value\ greater\ than\ X}{Number\ of\ benign\ lesions} \quad (23)$$

Sensitivity and specificity were used to evaluation the cutoff ADC value of malign lesions.

5. RESULTS

In this thesis four different studies were performed: Comparison of mean ADC values of benign and malign lesions, repeatability of ADC measurements, correlation between SNR and ADC values, and effect of lesion size to ADC values. The results of these studies are introduced next.

5.1 Comparison of mean ADC values

ADC values of lesions were measured as described in Chapter 4.3.1. Malign suspect were excluded from statistical analysis due to small sample size. ADC values of lesions were normalized by dividing the ADC value of lesions with ADC values of reference tissue. The distribution of original ADC values of 48 malign and 8 benign lesions is shown in Figure 12 and normalized ADC values in Figure 13. Also box plot is included.

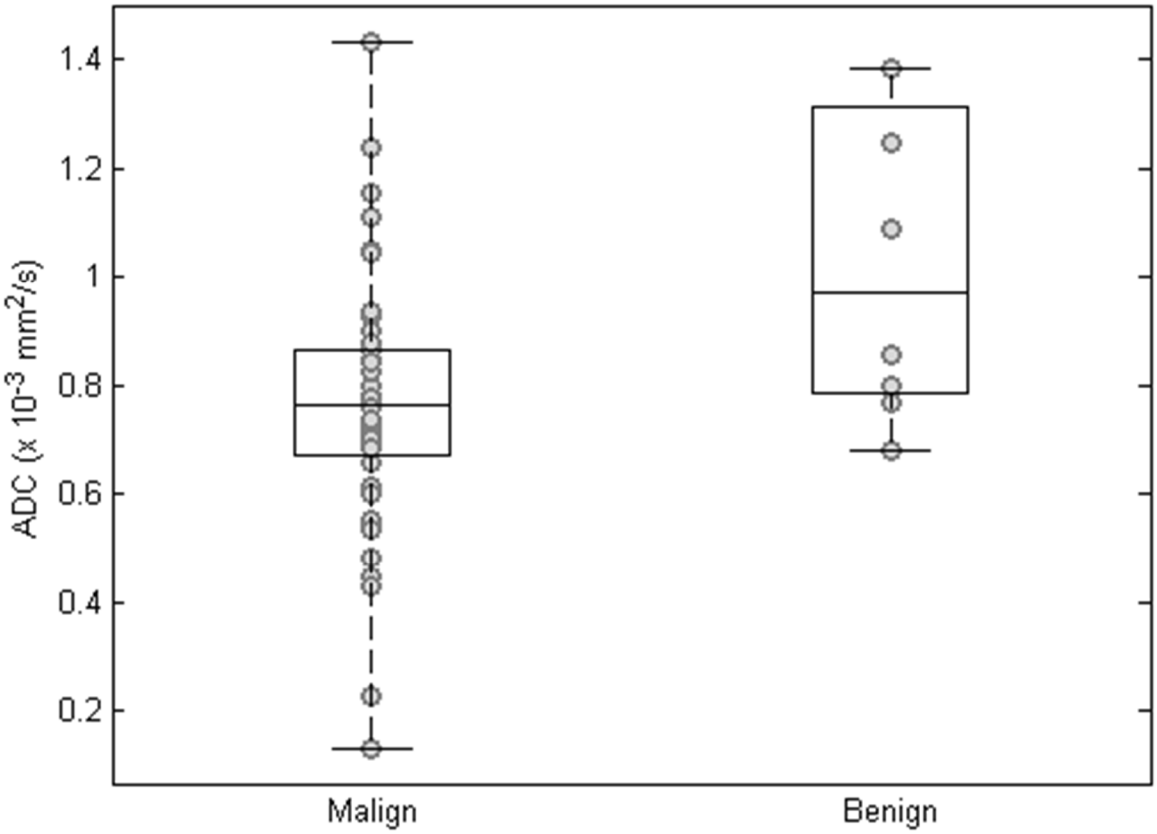

Figure 12. Measured ADC values of malign and benign lesions. Box plot shows the median of the sample (middle line inside the box) and 25 to 75 percentiles of data. The whiskers represent the minimum and maximum of the sample, i.e. range of values.

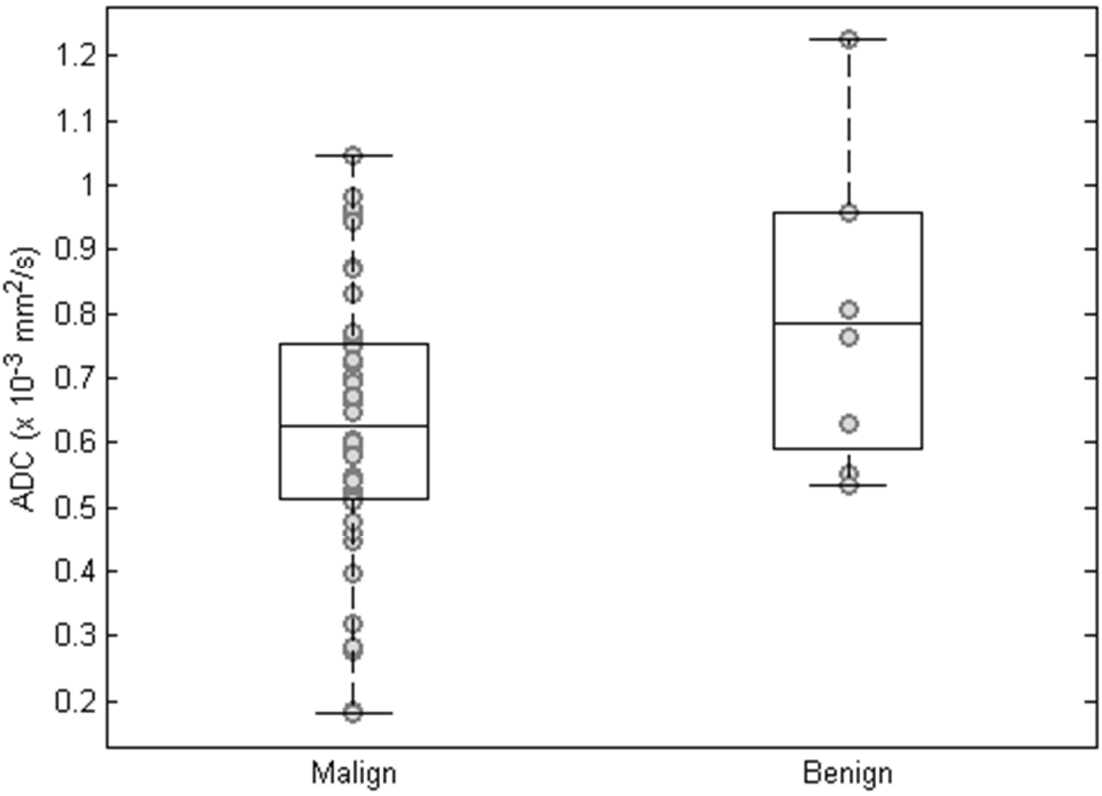

Figure 13. Normalized ADC values of malign and benign lesions. Box plot shows the median of the sample (middle line inside the box) and 25 to 75 percentiles of data. The whiskers represent the minimum and maximum of the sample, i.e. range of values.

It can be seen in Figure 12 and 13 that ADC values of malign and benign lesion overlap. The normalization makes the box plot of malign sample narrower. The benign sample distribution does not change much in normalization. The statistical information of the data is also gathered in to Table 5.

Table 5. Statistical information of the ADC measurement.

Type of lesion	**Number of lesions**	**ADC values**		**Normalized ADC values**	
		Range ($x10^{-3}$ mm^2/s)	Mean ($x10^{-3}$ mm^2/s)	Range ($x10^{-3}$ mm^2/s)	Mean ($x10^{-3}$ mm^2/s)
Benign	8	0.68 – 1.38	1.03 ± 0.29	0.54 - 1.23	0.80 ± 0.23
Malign	48	0.130 – 1.43	0.76 ± 0.23	0.18 - 1.05	0.63 ± 0.20

Normal distribution of the ADC values was tested with Kolmogorov-Smirnov separately for benign and malign samples. Both normalized and not normalized data were considered as normally distributed, with significance level 0.05 test (Table 6). The statistical significance of difference between malign and benign means was tested with *Independent-Samples' t test*. The malign and benign lesions ADC value means were signifi-

cantly different for both normalized (0.03) and not normalized cases (0.01) with significance level of 0.05. These results are presented in Table 6.

Table 6. Results for testing significance of benign and malign mean difference.

Statistical test		**Significance**	
		Not normalized	Normalized
Kolmogorov-Smirnov test	Benign	0.08	0.20
	Malign	0.20	0.20
Independent-Samples T test		0.01	0.03

5.2 Repeatability of ADC measurement

ADC measurements were repeated for 16 randomly chosen malign lesions. The measurement results for real ADC values are shown in Figure 14 and for normalized ADC values in Figure 15. Old measurement results from corresponding 16 lesions are plotted beside for comparison.

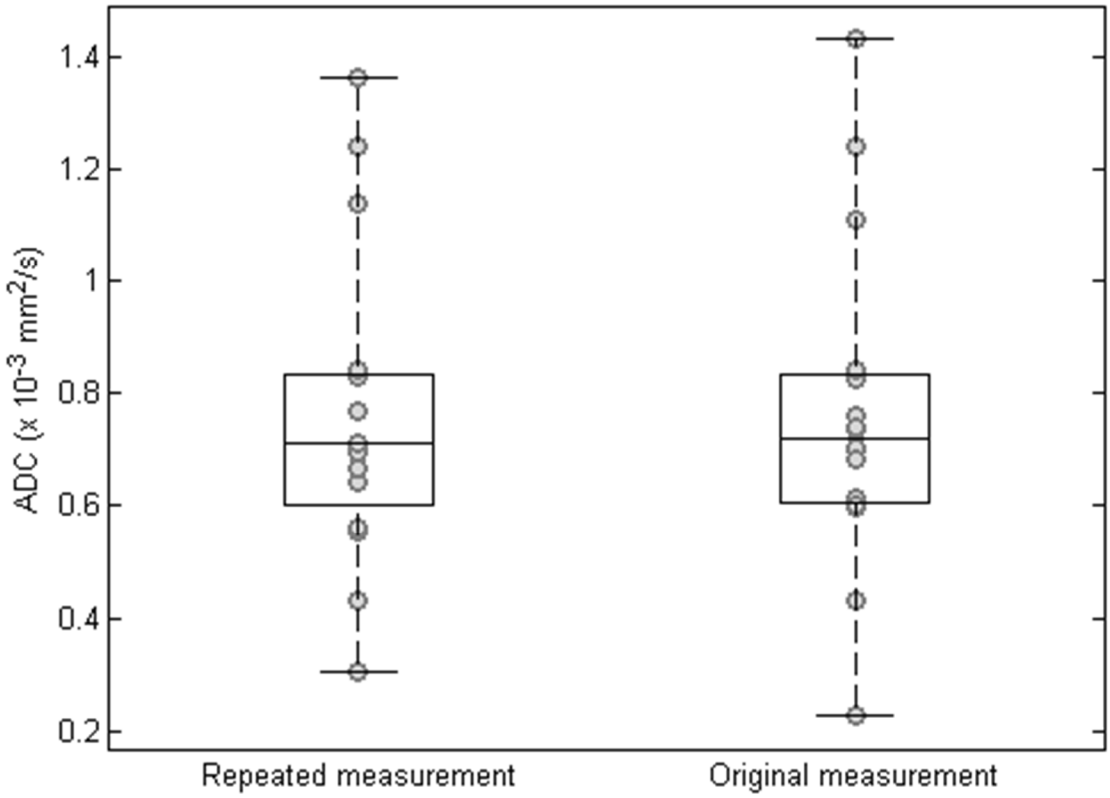

Figure 14. ADC values from repeated measurement on left and for comparison the corresponding ADC values from original measurement on right. Box plot shows the median of the sample (middle line inside the box) and 25 to 75 percentiles of data. The whiskers represent the minimum and maximum of the sample, i.e. range of values.

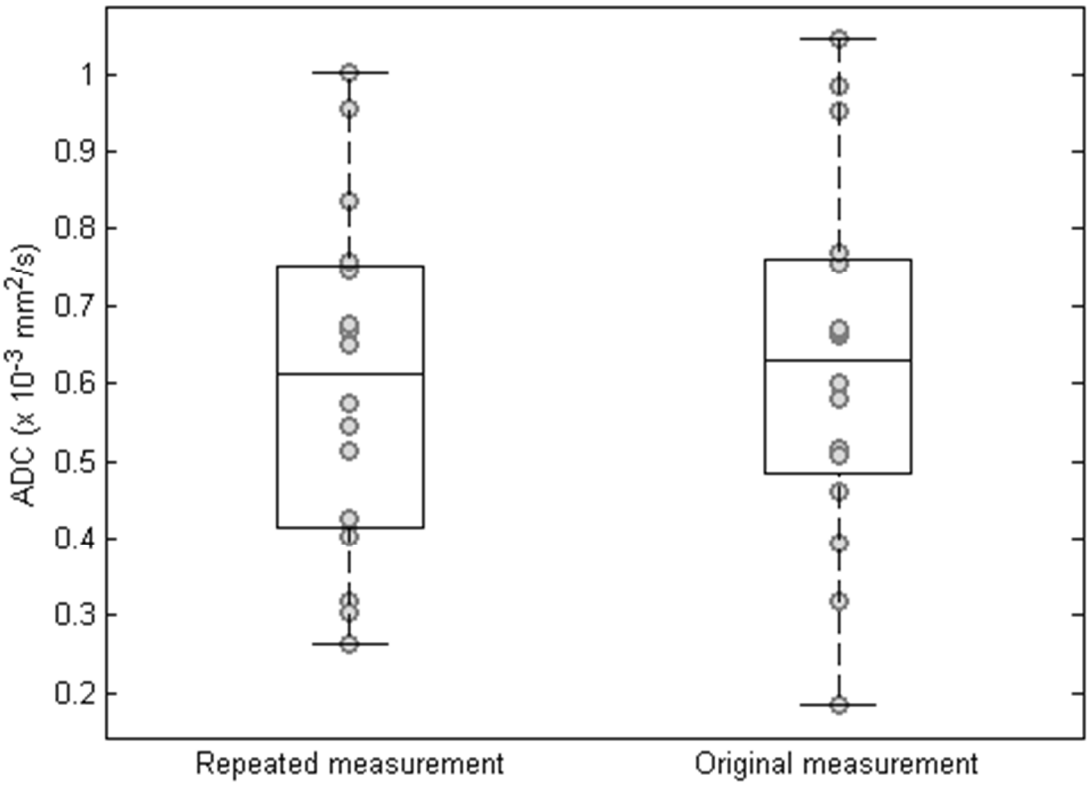

Figure 15. Normalized ADC values from repeated measurement on left and for comparison the corresponding ADC values from original measurement on right. Box plot shows the median of the sample (middle line inside the box) and 25 to 75 percentiles of data. The whiskers represent the minimum and maximum of the sample, i.e. range of values.

From Figures 14 and 15 can be seen that the medians lie at same levels both in original and repeated measurements and distributions and ranges of samples are similar. Normalization makes the box plot wider i.e. ADC values spread around median a little. The statistical information of these measurements is collected into Table 7.

Table 7. Statistical information of the repeatability measurement

Measurement	**ADC values**		**Normalized ADC values**	
	Range ($x\ 10^{-3}\ mm^2/s$)	Mean ($x10^{-3}\ mm^2/s$)	Range ($x10^{-3}\ mm^2/s$)	Mean ($x10^{-3}\ mm^2/s$)
Original	0.23 – 1.43	0.77	0.18 - 1.04	0.63
Repeated	0.30 – 1.36	0.76	0.26 - 1.00	0.60

The normal distribution of old and new ADC values of lesions was tested with Kolmogorov-Smirnov test. Both old and repeated samples (normalized and not normalized) were considered normally distributed (Table 8) with significance level 0.05. The reliability of the repeated measurements was tested with ICC values and the reliability

test was performed with absolute agreement. ICC value for not normalized data was found 0.99 and for normalized 0.94 (Table 8). Thus repeatability was excellent.

Table 8. Results for statistical reliability test.

Statistical test		**Significance**	
		Not normalized	Normalized
Kolmogorov-Smirnov test	Old meas.	0.06	0.20
	Repeated meas.	0.03	0.20
Reliability test		0.99	0.94

5.3 Correlation between SNR and ADC values

The mean SNR value was determined with equation (17) from 19 $b=0$ s/mm^2 DW images. The obtained SNR value was 40.6 ± 15.6.

SNR values were compared with ADC values of 19 random lesions (the original ADC values, not repeated measurements). The true ADC values were used, i.e. not normalized values. Comparison was performed with correlation calculation in *SPSS* software. First the normality of ADC value distribution was tested with Kolmogorov-Smirnov test and both variables were considered as normally distributed with significance level 0.05 (Table 9).

Table 9. Normal distribution test for ADC and SNR values

Kolmogorov-Smirnov Test	**ADC**	**SNR**
Significance	0.08	0.20

Next the actual correlation was tested with a *correlation matrix*, shown in Table 10. The correlation coefficient between ADC and SNR was positive (correlation coefficient 0.49) and statistically significant (significance level 0.05). The not normalized and normalized ADC values are also plotted against SNR values in Figures 16 and 17, respectively.

Table 10. Correlation matrix for ADC and SNR values

Correlation matrix, N=19		**ADC**	**SNR**
ADC	Pearson Correlation Significance	1 -	0.49 0.03
SNR	Pearson Correlation Significance	0.49 0.03	1 -

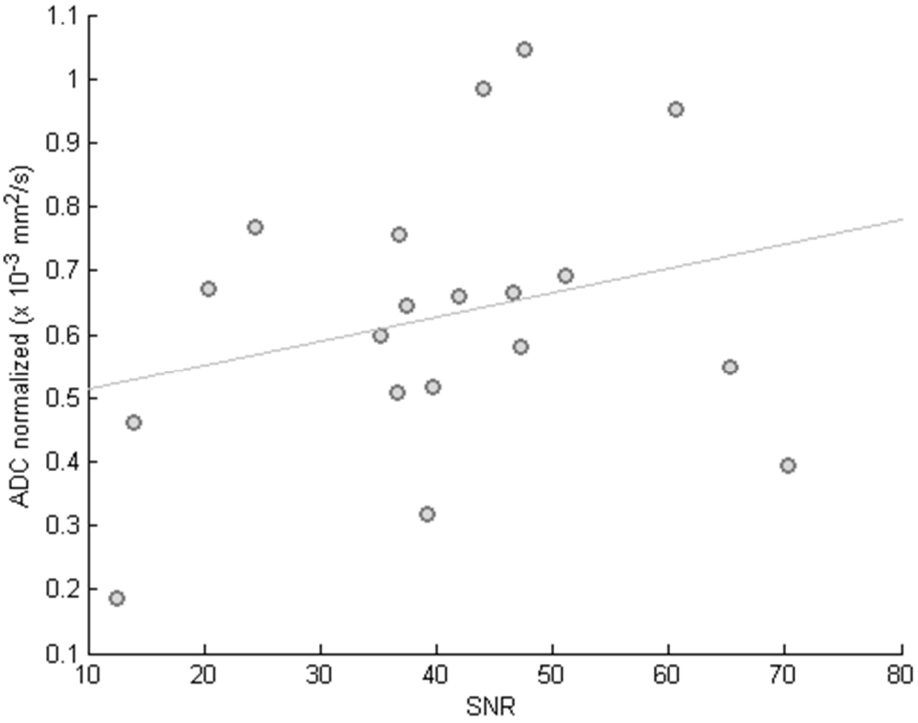

Figure 16. Graphical presentation of correlation between SNR and not normalized ADC values. Line shows least square fit for correlation.

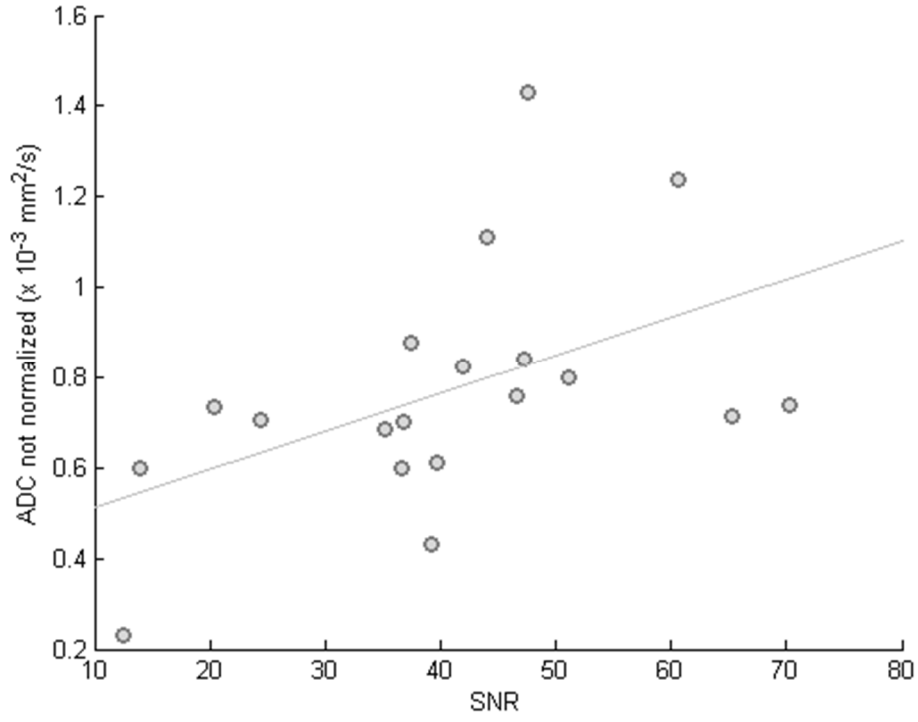

Figure 17. Graphical presentation of correlation between SNR and normalized ADC values. Line shows least square fit for correlation.

From Figure 16 and 17 can be seen that there is a slight trend that ADC values increase while SNR values increase. However, like the correlation coefficient (0.49) shows, the correlation is not very strong, because it is far away from unity.

5.4 Effect of lesion size to ADC values

Effect of lesion size to ADC values was tested with the repeated measurements. The ICC values were calculated for different lesion size groups: small, medium, and large. It was seen that ICC increased with increasing lesion size (Table 11.)

Table 11. ICC results for three different size groups of lesions.

Size group	Size range (mm^2)	N	ICC	
			Not normalized	Normalized
small	0.21-0.24	5	0.96	0.81
medium	0.31-0.51	6	0.99	0.92
large	0.67-1.45	5	0.995	0.98

Similarly with previous chapter, the correlation between lesion size and ADC values was analysed with correlation matrix. The normal distribution of data was already tested in part 5.1. The correlation was tested for both not normalized and normalized ADC values, shown in correlation matrix (Table 12).

Table 12. Correlation matrix for area, normalized and not normalized ADC values.

Correlation matrix, N=48		Area	ADC, not normalized	ADC, normalized
Area	Pearson Correlation	1	0.22	0.15
	Significance	-	0.14	0.30
ADC, not normalized	Pearson Correlation	0.22	1	0.80
	Significance	0.14	-	0.00
ADC, normalized	Pearson Correlation	0.15	0.80	1
	Significance	0.30	0.00	-

Lesion size and ADC values show poor correlation for both normalized (0.15) and not normalized ADC values (0.22). Moreover, results are not statistically significant (>0.05). Consequently, according to this study, no correlation can be seen between lesions size and ADC values. In Figures 18 and 19 the not normalized and normalized ADC values are plotted against lesion size.

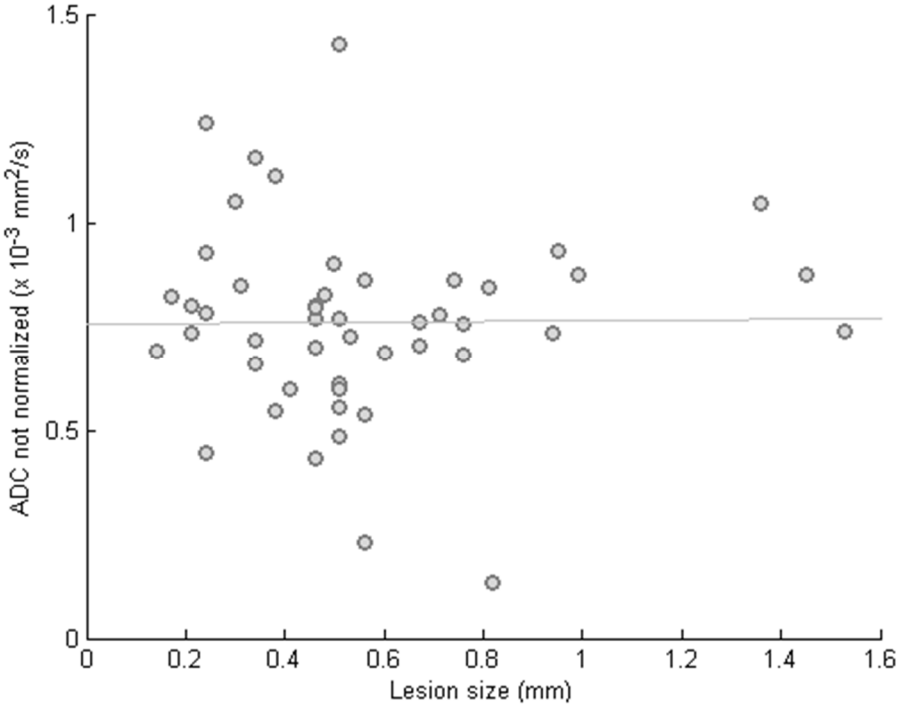

Figure 18. Graphical presentation of correlation between lesion size and not normalized ADC values. Line shows least square fit for correlation.

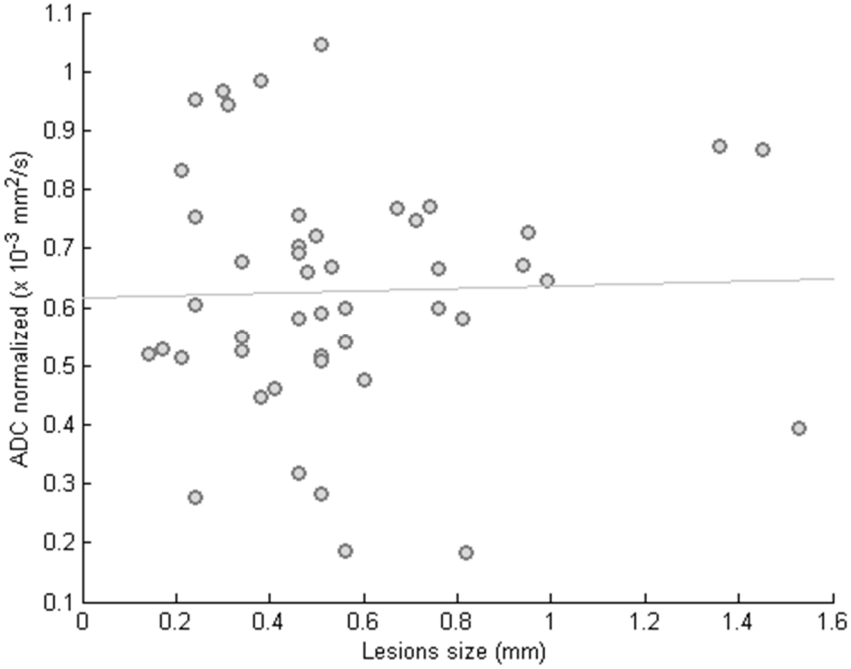

Figure 19. Graphical presentation of correlation between lesion size and normalized ADC values. Line shows least square fit for correlation.

Figures 18 and 19 support the result of correlation matrix. There is not any correlation between ADC and lesion size.

6. DISCUSSION

Diffusion-weighted imaging offers the potential novel contrast mechanism in MR imaging. Significant advantage of DWI over traditional contrast-enhanced MRI is its high sensitivity to change in microscopic water diffusion without the need for intravenous contrast material injection. Application of DWI in breast cancer diagnostics has been reported widely [34; 40; 42; 43; 53]. These studies show that mean ADC values of malignant tumours are significantly lower compared to benign lesions. Thus DWI is promising tool for breast cancer characterization. [7; 18] In this chapter the results introduced in previous chapter are discussed. Moreover, the criticisms towards the measurement and towards the method in general are presented. Finally, the clinical challenges and future prospects are discussed.

6.1 Results

Four different studies were performed: Comparison of mean ADC values of benign and malign lesions, repeatability of ADC measurements, correlation between SNR and ADC values, and effect of lesion size to ADC values. The results are collected here and discussed.

Comparison of mean ADC values

The mean normalized ADC values were measured to be $0.80 \pm 0.23 \times 10^{-3}$ mm^2/s for benign lesions and $0.63 \pm 0.20 \times 10^{-3}$ mm^2/s for malign lesions and there means were found to be statistically significantly different. These ADC values are considerably lower than values found in literature (Table 1). The results in Table 1 are mainly obtained with two different b-values and in this study the images were produced with four b-values ($b=0$, 50, 500, and 1500 s/mm^2). But according to study of *Bogner et al.* [35] this should not affect the ADC values this dramatically. Studies listed in Table 1 do not explain in detail the reasons for choice of reference point in tissues. This might be one differing factor affecting the dissimilarity in result.

Marini et al. [40] defined various threshold values for benign and malign lesion in their study. They for example defined thresholds as $mean_{benign}$ *-1 SD* and $mean_{benign}$ *+ 2 SD*. With modification to their method, the cutoff value for malign lesions was determined in this study to be $mean_{benign} + 1\ SD = 0.83 \times 10^{-3}$ mm^2/s. With this cutoff value the sensitivity of the method here was 83.3% and specificity of 37.3%. The low value of specificity is not very promising, but like was previously said, the benign sample was really small.

Repeatability of ADC measurements

In repeatability measurements the mean ADC value for malign lesion was obtained to be 0.60 x 10^{-3} mm^2/s. The repeatability was found excellent: the intra-class correlation was found 99.3 for not normalized ADC values and 94.4 for normalized values. This is in good line with study of *O'Flynn et al.* [54] who found ICC value of 0.93 for reproducibility of breast lesion ADC measurements.

The lower ICC value with normalized values was predictable. The lesion position is relatively easy to find with the help of DCE-MRI images, but the location of reference point depends how the measurer happens to determine it. Often reference ROI was also measured from different slice than the actual lesion ROI, which increases the inaccuracy in repetition.

Correlation between SNR and ADC values

The mean SNR value of $b=0\ s/mm^2$ images was determined to be 40.6 ± 15.6. *Mukherjee et al.* [55] suggest that SNR of the $b=0\ s/mm^2$ images of DTI acquisition should be at least 20 in order to determine reliable measures of parameters such as FA (equation 15) in brain structures. This can be used as suggestive value also for breast tissue which implies that the obtained result for SNR is good. In the correlation study between SNR and ADC values only poor correlation was discovered with correlation coefficient of 0.49 while best correlation is described with unity. Scatter plots (Figures 16 and 17) support this obtained correlation coefficient value: there is only slight positive trend between SNR and ADC values.

Effect of lesion size to ADC values

Effect of lesion size to ADC values was studied in two ways: ICC values in three different size groups (Table 11) and with correlation matrix (Table 12). The ICC values increased with lesion size in all three size groups. This makes sense because larger lesions are easier to distinguish in ADC maps and so also ROIs are easier to draw into same locations. ICC values with normalized ADC was smaller than with not normalized ADC values. Again this can be explained with the difficulty with reference point repeatability. The correlation matrix (Table 12) and scatter plots (Figure 18 and 19) showed that ADC values were not dependent on lesions size. This means that for example large lesions does not have stronger intensity in ADC maps than small lesions.

6.2 Reliability of the measurements

The studies performed had several limitations. First, the number of benign lesion (only eight) was very small to make reliable statistical analysis. In other studies [36-38; 40-

43] sample sizes have been over 20 for benign and malign lesions, like can be seen in Table 1. Moreover, in this study the benign lesions were not classified so the benign samples could have included any type of benign lesions. Therefore the obtained mean ADC of benign lesions would also depend on the different histological types included in the analysis.

Second, the ROI placement in ADC map affected significantly on measured ADC values. Even a small shift on ADC map could change ADC value dramatically and lead to false measurement result. Especially in the case of small lesions the accurate location of ROI on ADC map was difficult and possible only with the help of DCE-MR image comparison. The results of repeatability measurements also support this; bigger lesions were had better repeatability. In many studies [40; 53; 56] lesions smaller than 1 cm in diameter are considered difficult to detect in ADC maps.

6.3 Challenges in clinical applicability of breast DWI

DWI in a promising tool for breast imaging, but there are many challenges and limitation that need to be considered before wider clinical usability. In this chapter the challenges related to imaging parameters and ADC measurement protocol are discussed.

Imaging challenges

One challenge related to DWI as an imaging technique is its limited Signal-to-noise ratio. Relatively good SNR is important for tissue contrast and accurate ADC measurement. A higher SNR can also be used to increase the spatial resolution of DW imaging, when the detection of small lesions is easier [31]. Methods to improve SNR include for example increasing of voxel size and increasing the number of averages. One important factor is the choice of b values. Higher b-values decrease the SNR [57] but on the other hand a higher b-value improves contrast resolution [7; 31].

One of the greatest technical challenges in DWI is the effect of macroscopic motion, while retaining the sensitivity to the microscopic motion [58]. Movement of patient causes image misregistration, which leads to false ADC values. Only way to avoid patient movement is to make sure that patient is lying in a comfortable position and to optimize imaging protocol so that imaging time is minimized. [18]

Like discussed in *chapter 3.3.4 - Imaging protocol optimization* DW imaging of breast is technically challenging due to its location: tissue-air interfaces at skin surface and at thorax give rise to susceptibility artefacts and high fat tissue content causes image artefacts. This is why good fat suppression technique and shimming are needed. Optimal fat suppression is important for good contrast between normal breast tissue and lesions in ADC map. [18] However, fat suppressions decreases signal in DW images and even the most optimal suppression techniques are imperfect. Fat signal that is not fully suppressed may appear to increase the relative signal strength at high b-value DWI because the nonfat tissues are losing signal as diffusion weighting increases, whereas the remaining fat signal is not affected by diffusion weighting. [7] Moreover, the ADC

values of lesions including fat content is varied depending the used fat suppression technique and may lead to misdiagnosis [59].

Challenges in ADC measurement

Hand-drawn ROI-based techniques have limitations and set challenges to DWI. Like found in this thesis and in several studies [53; 56], ROI placement in ADC map is really critical and gives rise to measurement errors. The obtained ADC values from hand-drawn ROIs depends greatly on the measurer so the reproducibility and comparison of different studies is complicated. Moreover, hand-drawn ROI-based techniques are time consuming. [7] Development of semiautomatic methods is needed for more reliable and comparable results. Some studies of this development are made [60] and the results seem promising. However, if DCE-MRI figures are used to help in lesion location, errors might arise in shifts in patient position between imaging sequences. [7]

The ADC value of breast tissue may be somewhat dependent of menstrual cycle phase. This variation arises from the change in water content in the breast tissue during the menstrual cycle. *Partridge et al* [61] found the variation of breast ADC to be 5.5% across different menstrual phases. Trend showed that decreased ADC values in the second week of cycle and a peak in ADC during the week prior to menstruation. However, other studies [54; 62] have not detect significant difference in ADC values during menstrual cycle.

6.4 Future prospects

Studies carried out in this thesis give promising results about breast DWI and thus it would be interesting to continue the studies. In the future it would be interesting to examine the optimization of ADC maps with different b-values. Also studies with several different malign lesion types would be natural next step.

In general DWI seems a promising tool for breast cancer imaging and characterization. The most significant advantage of DW imaging over traditional contrast-enhanced MR imaging is its high sensitivity in the detection of breast cancer. DW imaging has strong potential as an adjunct MR imaging technique to reduce false positive results and unnecessary biopsies. This tumor characterization method is the most studied application of DW imaging. [7; 18]

In addition to this, screening MR imaging of breast without added contrast material is a prospective application for DW imaging. Conventional screening with DCE-MRI is highly sensitive for identification of lesions but it is not suitable for all patients; used gadolinium-based contrast material is associated with nephrogenic systemic fibrosis [63]. Moreover, DCE-MRI is more time consuming and expensive than DWI of the breast. Nevertheless, the potential of DWI as a noncontrast alternative for DCE-MRI screening method been only little studied so it needs further examination. [7; 18]

DWI has also potential in predicting the effect of *neoadjuvant chemotherapy* [64; 65]. Tumor response is typically measured by change in size but alternative mark-

ers such as tumor cellularity, vascularity, or rate of cell proliferation are possible measurable variables with DWI. ADC value may provide an earlier biomarker for tumor response. Early prediction of the effect of chemotherapy would allow timely optimization of the therapy protocol to ensure the best therapeutic effect. [7; 18]

Before wide clinical use the standard protocol for DW breast imaging has to be agreed; results obtained around the world needs to be comparable. For example choice of b-values and number of them affect significantly on the obtained ADC values [31; 35]. Moreover, if DWI is used along with DCE-MRI the effect of contrast agent to the ADC values needs to be taken into account; studies [66; 67] show that ADC values are lower if DWI is performed after contrast enhancement. *Firat et al* [67] suggest that at least 6-10 min delay is preferable before DW imaging, which is not favoured in clinical use: it increases the imaging time and may lead to position shifts between imaging sequences. This is why DW imaging is usually performed before the contrast-enhanced imaging. And like discussed in *chapter 6.3 –Imaging challenges* the used fat suppression technique also affect into the measured ADC values so it needs to be standardized as well. And of course the ADC value normalization method needs universal guidelines so that measurement results are comparable.

7. CONCLUSION

In this Master of Science thesis the ADC values of malign and benign breast lesions were examined through four studies: Comparison of mean ADC values of benign and malign lesions, repeatability of ADC measurements, correlation between SNR and ADC values, and effect of lesion size to ADC values. In the measurements the breast tissue changes of 45 patients (age range 45-83 years) were used. These changes included 48 ductal carcinomas in situ and 8 benign changes.

The normalized mean ADC values for benign lesions was found $0.80 \pm 0.23 \times 10^{-3}$ mm^2/s and for malign lesions $0.63 \pm 0.20 \times 10^{-3}$ mm^2/s and they were found significantly different. The cutoff value for malign lesions was determined 0.83×10^{-3} mm^2/s with sensitivity of 83.3% and specificity of 37.3%. The measurement method showed excellent repeatability, especially with big lesions. ADC and SNR values were not found to be correlated with each other.

The results of this thesis were promising and in line with the literature values. The obtained cutoff value has the best direct clinical applicability: radiologists can use it as a guidance tool in breast cancer evaluation. It tells that when ADC value of lesion is less than 0.83 the lesions can be strongly considered as malign and when ADC value is greater than 0.83, it is strongly benign. This is valuable information for example when doctor is considering the need for further imaging or histological biopsies.

Overall DWI is a potential imaging method for oncological applications. It enables the lesions characterization with its microscopic diffusion sensitive imaging sequence. In breast cancer imaging DWI has multiple advantages over conventional contrast-enhanced MRI, for example it is cheaper and faster than DCE-MRI and to top it all it increases the sensitivity of breast lesion characterization.

REFERENCES

[1] Weishaupt, D., Köchli, V.D. & Marincek, B. How Does MRI Work? An Introduction to the Physics and Function of Magnetic Resonance Imaging. 2nd ed. Berlin, Germany 2008, Springer. 169 p.

[2] Bushberg, J.T. The essential physics of medical imaging. 3rd ed. Philadelphia 2012, Wolters Kluwer Health/Lippincott Williams & Wilkins, 1030 p.

[3] Luna, A., Ribes, R. & Soto, J.A. Diffusion MRI Outside the Brain : A Case-Based Review and Clinical Applications. 2012, Springer, Berlin, Germany, 400p.

[4] American Cancer Society Breast Cancer. 2014, American Cancer Society. Cited 9.2.2015. Available at: www.cancer.org/acs/groups/cid/documents/webcontent/003090-pdf.pdf

[5] Mäkinen, M., Carpén, O., Kosma, V., Lehto, V., Paavonen, T. & Stenbäck, F. Patologia. 2012, Duodecim, Helsinki, Finland 1261 p.

[6] Joensuu, H., Roberts, P.J., Kellokumpu-Lehtinen, P., Jyrkkiö, S., Kouri, M. & Lyly, T. Syöpätaudit. 5th ed. 2013, Duodecim, Helsinki, Finland. 1032 p.

[7] Partridge, S.C. & McDonald, E.S. Diffusion Weighted Magnetic Resonance Imaging of the Breast: Protocol Optimization, Interpretation, and Clinical Applications. Magnetic resonance imaging clinics of North America 21(2013)3, pp. 601-624.

[8] Elmaoglu, M. & Çelik, A. MRI Handbook: MR Physics, Patient Positioning, and Protocols. Springer, New York, USA, 2012, 318 p.

[9] McRobbie, D.W., Moore, E.A., Graves, M.J. & Prince, M.R. MRI From Picture to Proton. Second ed. New York 2006, Cambridge University Press. 393 p.

[10] Smith, N.B. & Webb, A. Introduction to Medical Imaging: Physics, Engineering and Clinical Applications. Cambridge, UK 2013, Cambridge University Press. 286 p.

[11] Mudry, K.M., Plonsey, R. & Bronzino, J.D. Biomedical Imaging. Boca Raton 2003, CRC Press. 360 p.

[12] Nelson, P.C. Biological physics: energy, information, life. New York 2004, W. H. Freeman. 598 p.

[13] Perrin, V. MRI Techniques. London, UK 2013, ISTE. 224 p.

[14] Hiltunen, J. Novel diffusion tensor imaging (DTI) approaches at 3T. Dissertation. Espoo 2013. Aalto University. Aalto University publication series Doctoral Dissertations 93/2013. 79 p.

[15] Hiltunen, J., Seppa, M. & Hari, R. Diffuusiotensorikuvaus hermoratojen tutkimuksessa. Duodecim 123(2007)15, pp. 1851.

[16] Hagmann, P., Jonasson, L., Maeder, P., Thiran, J., Wedeen, V.J. & Meuli, R. Understanding Diffusion MR Imaging Techniques: From Scalar Diffusion-weighted Imaging to Diffusion Tensor Imaging and Beyond. RadioGraphics 26(2006) pp. S205-S223.

[17] Bonekamp, S., Corona-Villalobos, C.P. & Kamel, I.R. Oncologic applications of diffusion-weighted MRI in the body. Journal of Magnetic Resonance Imaging 35(2012)2, pp. 257-279.

[18] Woodhams, R., Ramadan, S., Stanwell, P., Sakamoto, S., Hata, H., Ozaki, M., Kan, S. & Inoue, Y. Diffusion-weighted Imaging of the Breast: Principles and Clinical Applications. RadioGraphics 31(2011)4, pp. 1059-1084.

[19] Masutani, Y., Aoki, S., Abe, O., Hayashi, N. & Otomo, K. MR Diffusion Tensor Imaging: Recent Advantage and New Techniques for Diffusion Tensor Visualization. European Journal of Radiology 46(2003) pp. 53-66.

[20] Koh, D. & Collins, D.J. Diffusion-Weighted MRI in the Body: Applications and Challenges in Oncology. American Journal of Roentgenology 188(2007)6, pp. 1622-1635.

[21] Dong, Q., Welsh, R.C., Chenevert, T.L., Carlos, R.C., Maly-Sundgren, P., Gomez-Hassan, D.M. & Mukherji, S.K. Clinical applications of diffusion tensor imaging. Journal of Magnetic Resonance Imaging 19(2004)1, pp. 6-18.

[22] Drake, R.L., Vogl, A.W. & Mitchell, A.W.M. Gray's Anatomy for Students. 2nd ed. Philadelphia 2010, Elsevier. 1103 p.

[23] Thomas, P.A. Breast Cancer and its Precursor Lesions: Making Sense and Making It Early (Current Clinical Pathology). New York 2011, Springer. 79 p.

[24] Kumar, V., Abbas, A., K. & Aster, J.C. Pathological Basis of Disease. 9th Edi-tion, Elsevier, Philadelphia. 2015. 1391 p.

[25] Lynch, P.J. Breast anatomy normal scheme. 8.3.2015, [cited 8.3.2015]. Available at: http://commons.wikimedia.org/wiki/File:Breast_anatomy_normal_scheme.png#mediaviewer/File:Breast_anatomy_normal_scheme.png.

[26] Kumar, V., Abbas, A.K. & Aster, J.C. Robbins Basic Pathology. 9th ed. Philadelphia 2013, Elsevier. 910 p.

[27] Ng, E.Y.K., Acharya, U.R., Rangayyan, R.M. & Suri, J.S. Multimodality Breast Imaging : Diagnosis and Treatment. Bellingham, Washington cop. 2013, SPIE Press, 542 s p.

[28] Standerskjöld-Nordenstam, C., Kormano, M., Laasonen, E.M., Soimakallio, S. & Suramo, I. Kliininen radiologia. Helsinki, FInland 1998, Duodecim. 404 p.

[29] Hunt, K.K., Robb, G.L., Strom, E.A. & Ueno, N.T. The MD Anderson Cancer Care Series: Breast Cancer. 2nd ed. New York 2008, Springer. 561 p.

[30] Hukkinen, K. Rintojen magneettikuvaus. 129(2013)20, pp. 2163.

[31] Thomassin-Naggara, I., De Bazelaire, C., Chopier, J., Bazot, M., Marsault, C. & Trop, I. Diffusion-weighted MR imaging of the breast: Advantages and pitfalls. European Journal of Radiology 82(2013)3, pp. 435-443.

[32] Rubesova, E., Grell, A., De Maertelaer, V., Metens, T., Chao, S. & Lemort, M. Quantitative diffusion imaging in breast cancer: A clinical prospective study. Journal of Magnetic Resonance Imaging 24(2006)2, pp. 319-324.

[33] Charles-Edwards, E.M. Diffusion-weighted magnetic resonance imaging and its application to cancer. Cancer Imaging 6(2006)1, pp. 135-143.

[34] Park, M.J., Cha, E.S., Kang, B.J., Ihn, Y.K. & Baik, J.H. The Role of Diffusion-Weighted Imaging and the Apparent Diffusion Coefficient (ADC) Values for Breast Tumors. Korean J Radiol 8(2007)5, pp. 390-396.

[35] Bogner, W., Gruber, S., Pinker, K., Grabner, G., Stadlbauer, A., Weber, M., Moser, E., Helbich, T.H. & Trattnig, S. Diffusion-weighted MR for Differentiation of Breast Lesions at 3.0 T: How Does Selection of Diffusion Protocols Affect Diagnosis? Radiology 253(2009)2, pp. 341-351.

[36] Abdulghaffar, W. & Tag-Aldeen, M.M. Role of diffusion-weighted imaging (DWI) and apparent diffusion coefficient (ADC) in differentiating between benign and malignant breast lesions. Egyptian Journal of Radiology and Nuclear Medicine 44(2013)4, pp. 945-951.

[37] Gouhar, G.K. & Zidan, E.H. Diffusion-weighted imaging of breast tumors: Differentiation of benign and malignant tumors. The Egyptian Journal of Radiology and Nuclear Medicine 42(2011)1, pp. 93-99.

[38] Guo, Y., Cai, Y., Cai, Z., Gao, Y.-., An, N., Ma, L., Mahankali, S. & Gao, J. Differentiation of clinically benign and malignant breast lesions using diffusion-weighted imaging. Journal of Magnetic Resonance Imaging 16(2002)2, pp. 172-178.

[39] Kuroki, Y., Nasu, K., Kuroki, S., Murakami, K., Hayashi, T., Sekiguchi, R. & Nawano, S. Diffusion-weighted Imaging of Breast Cancer with the Sensitivity Encoding Technique: Analysis of the Apparent Diffusion Coefficient Value. Magnetic Resonance in Medical Sciences 3(2004)2, pp. 79-85.

[40] Marini, C., Iacconi, C., Giannelli, M., Cilotti, A., Moretti, M. & Bartolozzi, C. Quantitative diffusion-weighted MR imaging in the differential diagnosis of breast lesion. European radiology 17(2007)10, pp. 2646-2655.

[41] Moukhtar, F.Z. & Abu El Maati, A.A. Apparent diffusion coefficient values as an adjunct to dynamic contrast enhanced MRI for discriminating benign and malignant breast lesions presenting as mass and non-mass like enhancement. Egyptian Journal of Radiology and Nuclear Medicine 45(2014)2, pp. 597-604.

[42] Spick, C., Pinker-Domenig, K., Rudas, M., Helbich, T.H. & Baltzer, P.A. MRI-only lesions: application of diffusion-weighted imaging obviates unnecessary MR-guided breast biopsies. European radiology 24(2014)6, pp. 1204-1210.

[43] Woodhams, R., Matsunaga, K., Kan, S., Hata, H., Ozaki, M., Iwabuchi, K., Kuranami, M., Watanabe, M. & Hayakawa, K. ADC Mapping of Benign and Malignant Breast Tumors. Magnetic Resonance in Medical Sciences 4(2005)1, pp. 35-42.

[44] Peters, N.H.G.M., Vincken, K.L., van den Bosch, M.A.A.J., Luijten, P.R., Mali, W.P.T.M. & Bartels, L.W. Quantitative diffusion weighted imaging for differentiation of benign and malignant breast lesions: The influence of the choice of b-values. Journal of Magnetic Resonance Imaging 31(2010)5, pp. 1100-1105.

[45] Kuroki, Y. & Nasu, K. Advances in breast MRI: diffusion-weighted imaging of the breast. Breast Cancer 15(2008)3, pp. 212-217.

[46] Pereira, F.P.A., Martins, G., Figueiredo, E., Domingues, M.N.A., Domingues, R.C., da Fonseca, L.M.B. & Gasparetto, E.L. Assessment of Breast Lesions With Diffusion-Weighted MRI: Comparing the Use of Different b Values. American Journal of Roentgenology 193(2009)4, pp. 1030-1035.

[47] Ravert, P.K. & Huffaker, C. Breast cancer screening in women: An integrative literature review. Journal of the American Academy of Nurse Practitioners 22(2010)12, pp. 668-673.

[48] Kolb, T.M., Lichy, J. & Newhouse, J.H. Comparison of the Performance of Screening Mammography, Physical Examination, and Breast US and Evaluation of Factors that Influence Them: An Analysis of 27,825 Patient Evaluations. Radiology 225(2002)1, pp. 165-175.

[49] Faber, M.H. Statistics and Probability Theory: In Pursuit of Engineering Decision Support. Springer, London, UK, 2012, 190 p.

[50] Riffenburgh, R.H. Statistics in medicine. 2nd ed. ed. Amsterdam cop. 2006, Elsevier Academic Press, 622 s p.

[51] Bartko, J.J. The intraclass correlation coefficient as a measure of reliability. Psychological reports 19(1966)1, pp. 3-11.

[52] Fisher, R.A. Statistical Methods for Research Workers. 5th ed. Edinburgh 1934, Oliver and Boyd. 378 p.

[53] Tan, S.L.L., Rahmat, K., Rozalli, F.I., Mohd-Shah, M.N., Aziz, Y.F.A., Yip, C.H., Vijayananthan, A. & Ng, K.H. Differentiation between benign and malignant breast lesions using quantitative diffusion-weighted sequence on 3 T MRI. Clinical radiology 69(2014)1, pp. 63-71.

[54] O'Flynn, E.A.M., Morgan, V.A., Giles, S.L. & de Souza, N.M. Diffusion weighted imaging of the normal breast: reproducibility of apparent diffusion coefficient measurements and variation with menstrual cycle and menopausal status. European radiology 22(2012)7, pp. 1512-1518.

[55] Mukherjee, P., Chung, S.W., Berman, J.I., Hess, C.P. & Henry, R.G. Diffusion tensor MR imaging and fiber tractography: technical considerations. AJNR.American journal of neuroradiology 29(2008)5, pp. 843-852.

[56] Hatakenaka, M., Soeda, H., Yabuuchi, H., Matsuo, Y., Kamitani, T., Oda, Y., Tsuneyoshi, M. & Honda, H. Apparent diffusion coefficients of breast tumors: Clinical application. Magnetic Resonance in Medical Sciences 7(2008)1, pp. 23-29.

[57] Woodhams, R., Inoue, Y., Ramadan, S., Hata, H. & Ozaki, M. Diffusion-weighted Imaging of the Breast: Comparison of B-values 1000 s/mm^2 and 1500 s/mm^2. Magnetic Resonance in Medical Sciences 12(2013)3, pp. 229-234.

[58] Bammer, R. Basic principles of diffusion-weighted imaging. European Journal of Radiology 45(2003)3, pp. 169-184.

[59] Breast DWI at 3 T: Influence of the fat-suppression technique on image quality and diagnostic performance. 2015, W.B. Saunders Ltd. pp. 286-294.

[60] Ma, B., Meyer, C.R., Pickles, M.D., Chenevert, T.L., Bland, P.H., Galbán, C.J., Rehemtulla, A., Turnbull, L.W. & Ross, B.D. Voxel-by-Voxel Functional Diffusion Mapping for Early Evaluation of Breast Cancer Treatment. In: Prince, J., Pham, D. & Myers, K. (ed.). 2009, Springer Berlin Heidelberg. pp. 276-287.

[61] Partridge, S.C., McKinnon, G.C., Henry, R.G. & Hylton, N.M. Menstrual cycle variation of apparent diffusion coefficients measured in the normal breast using MRI. Journal of Magnetic Resonance Imaging 14(2001)4, pp. 433-438.

[62] EI Khouli, R.,H., Jacobs, M.A., Mezban, S.D., Huang, P., Kamel, I.R., Macura, K.J. & Bluemke, D.A. Diffusion-weighted Imaging Improves the Diagnostic Accuracy of Conventional 3.0-T Breast MR Imaging. Radiology 256(2010)1, pp. 64-73.

[63] Agarwal, R., Brunelli, S.M., Williams, K., Mitchell, M.D., Feldman, H.I. & Umscheid, C.A. Gadolinium-based contrast agents and nephrogenic systemic fibrosis: a systematic review and meta-analysis. Nephrology Dialysis Transplantation 24(2009)3, pp. 856-863.

[64] Sharma, U., Danishad, K.K.A., Seenu, V. & Jagannathan, N.R. Longitudinal study of the assessment by MRI and diffusion-weighted imaging of tumor response in patients with locally advanced breast cancer undergoing neoadjuvant chemotherapy. NMR in biomedicine 22(2009)1, pp. 104-113.

[65] Pickles, M.D., Gibbs, P., Lowry, M. & Turnbull, L.W. Diffusion changes precede size reduction in neoadjuvant treatment of breast cancer. Magnetic resonance imaging 24(2006)7, pp. 843-847.

[66] Yuen, S., Yamada, K., Goto, M., Nishida, K., Takahata, A. & Nishimura, T. Microperfusion-induced elevation of ADC is suppressed after contrast in breast carcinoma. Journal of Magnetic Resonance Imaging 29(2009)5, pp. 1080-1084.

[67] Firat, A.K., Sanh, B., Karakas, H.M. & Erdem, G. The effect of intravenous gadolinium-DTPA on diffusion-weighted imaging. Neuroradiology 48(2006)7, pp. 465-470.